ASSESSMENT OF POTENTIAL COMMERCIAL SUCCESS OF BUSINESS JETS WITH NATURAL LAMINAR FLOW TECHNOLOGY

Stanislav Karpuk, Ali Elham[1]

[1] Institute of Aircraft design and Lightweight Structures, Technical University Braunschweig, Braunschweig, Germany

Abstract

The present research investigates the potential application of the Natural Laminar Flow (NLF) wing technology to business jet market segments from light to large jets. A database of existing business jets was generated to determine the range extension as a potential driver of customer interest. A conceptual design of several configurations for each market segment that satisfies Top-level Requirements of reference aircraft was performed to investigate potential improvements of the aircraft flight range, operating costs, and changes in acquisition prices using the NLF technologies. An initial sizing module within SUAVE and a low-fidelity multi-disciplinary design optimization tool were used to size all aircraft configurations. Potential configurations included a classical backward-swept aft-fuselage mounted engines configuration, configurations with forward-swept wings, and variations with wing-mounted engines. Results demonstrated 5-15% increase in the flight range depending on the aircraft concept and a substantial increase in productivity for larger aircraft. A rapid increase in acquisition prices suggested that only super mid-size jets that combine relatively low empty weight and high range extension potential may be potentially successful in the market, but technology needs to have sufficient maturity to allow this potential.

Keywords: Aircraft Design, Natural Laminar Flow, Business jet

1. Introduction

The business jet market is a relatively small but highly competitive arena. Every manufacturer is continuously working on aircraft performance and systems improvements to offer maximum customer comfort with the best flying capabilities. Present improvements of modern business jets are mostly related to improvements of systems for passenger comfort and safety, avionics, and flight control systems. Similar to commercial aircraft, modern business jets are approaching their performance limits since existing technologies, and the aircraft configuration which features them has been developed for a significant amount of time. More advanced airframe technologies are not only challenging from the development standpoint but also introduce significant risks to a manufacturer in terms of potential returns of investments into an aircraft with one or several unconventional technologies.

From the perspective of a commercial jetliner, minimum possible operating costs with maximum possible performance are of major interest for airlines and are a major goal of aircraft manufacturers. In addition, current research and development have also started focusing on technologies dedicated towards more environmentally-friendly aircraft ranging from regional aircraft to long-range commercial jets. For business aviation, operating costs are also important, but aircraft performance becomes a more valuable characteristic since business aviation is dedicated to customers that can afford to spend extra money for their transportation convenience. Consequently, new technologies for business aircraft may have success in the business aviation market if they provide significant performance or passenger experience improvement and are not extremely expensive for the manufacturer to mitigate risks related to the program's success. In addition, new airframe or propulsion technologies that

are commercially interesting for large passenger jets may not necessarily be viable for the business aviation market.

A widely used metric for the business jet performance evaluation is the Productivity Index (PI), defined by

$$PI = \frac{R_{LRC}M_{LRC}V_{cab}}{TOFL} \tag{1}$$

where R_{LRC} is the range at the long-range cruise speed (payload of 4 passengers (PAX) for very light to large categories and six passengers for ultra-long-range jets), M_{LRC} is the long-range cruise Mach number, V_{cab} is the cabin volume excluding the cockpit and the baggage volume, and $TOFL$ is the take-off field length. Combined with the aircraft price, the relation between the two values can be generated and used as a metric for the aircraft value (where higher PI with lower price is a more valuable aircraft) and comparison among several aircraft. Figure 1 shows a sample curve of PI indices and equipped prices for various business aircraft.
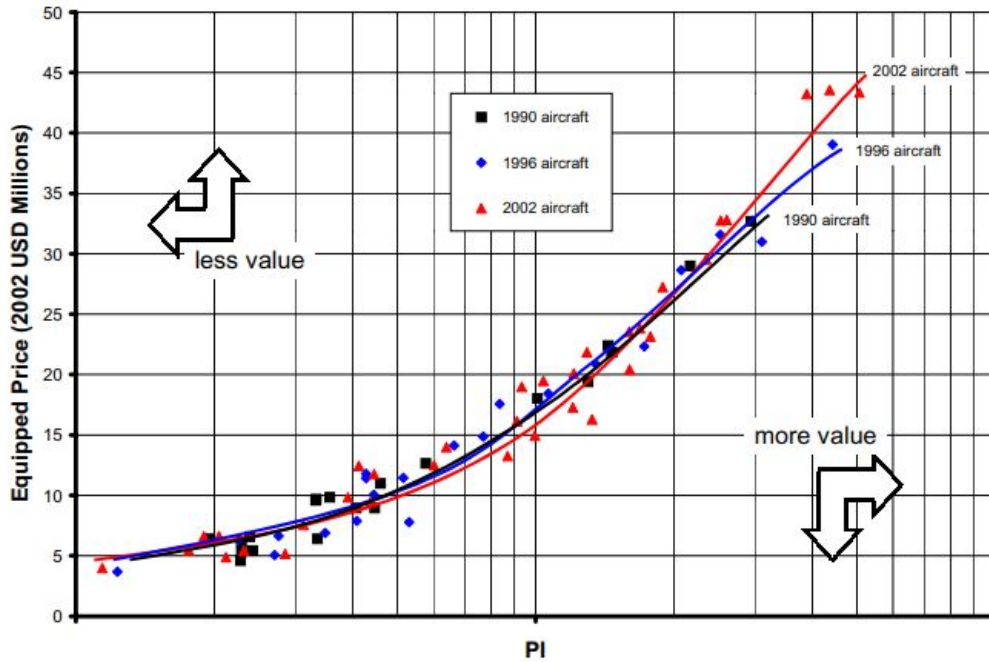
Figure 1 – Business Aircraft Productivity Index versus Price for 1990, 1996 and 2000 [1].

For commercial jets, the PI can be defined according to Isikveren [1] by

$$PIC = \frac{R_{LRC}M_{LRC}V_{cab}N_{PAX}}{TOFL} \tag{2}$$

where the additional variable N_{PAX} corresponds to the number of passengers in the standard configuration. It is evident from Eq. 1 and Eq. 2 that although both relations share similar productivity parameters, the difference in formulations affects individual contributions of each parameter to the overall PI. Moreover, changes in individual contributions of PI parameters may also affect the usefulness of new technologies for each market.

For commercial aircraft, aircraft and engine manufacturers are continuously improving technologies to maximize aircraft fuel efficiency. From the airframe perspective, reduction in zero-lift drag (C_{D_0}) is one of the major contributors toward a more fuel-efficient aircraft which can reduce both the environmental impact by reduced emission and its Direct Operating Costs (DOC) due to less required fuel if the drag reduction technology is not excessively expensive to maintain. From the business-jet market perspective, reduction in drag may enable the aircraft to extend its range without an increase in DOC, which will directly affect the PI and potential customer interest in the aircraft compared to existing competitors.

Extension of the laminar flow around the aircraft can significantly reduce the C_{D_0} and increase the aircraft fuel efficiency. The aircraft laminar boundary layer can be extended in two ways: aerodynamic
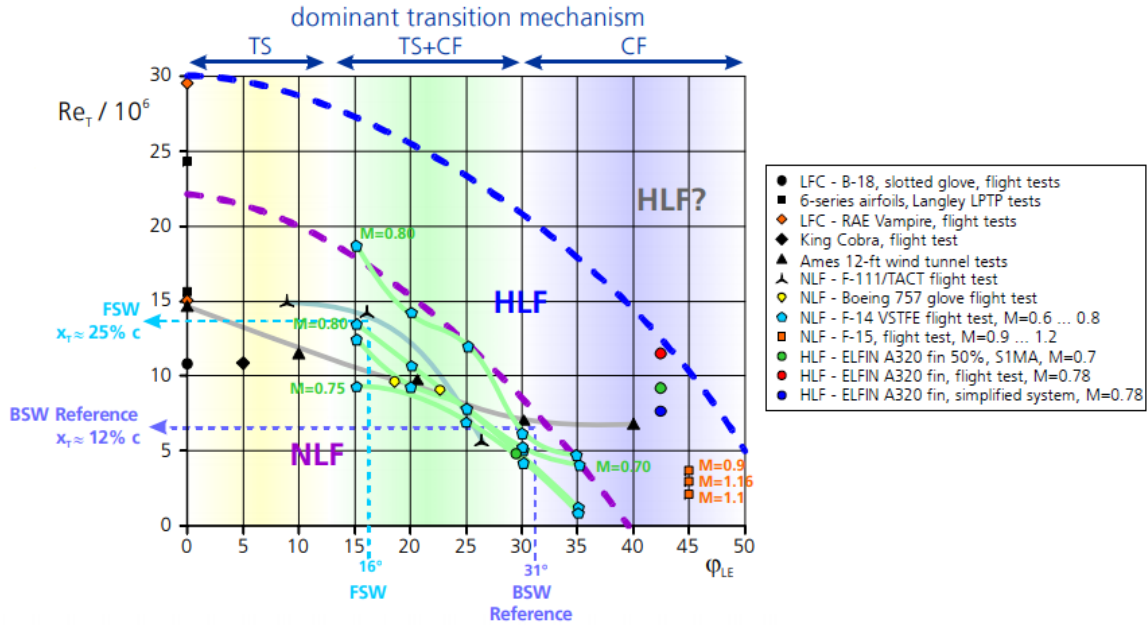
Figure 2 – Boundaries of NLF and HLF as a function of the leading edge sweep (ϕ_{LE}) and transition Reynolds number (Re_T) with experimental data [2].

shaping of the lifting surface to delay the adverse pressure gradient as much as possible to achieve a natural laminar flow (NLF) or to actively flow control (AFC) where the boundary layer suction is applied to delay the transition. Two approaches can also be combined to have a hybrid laminar flow control (HLFC) approach. Both AFC and NLF methods have their benefits and drawbacks. While the AFC can virtually keep the flow laminar as long as required if sufficient energy is applied, the system integration and structural design of the airframe with such systems is excessively complex and is currently limited to research airplanes for flight-test experiments [3]. The NLF, however, relies only only on the aerodynamic shaping of the airframe and its smoothness. However, achieving exceptionally smooth surface quality is a challenging task, given that roughness created by the deicing/anti-icing system, skin waviness, and foreign objects such as dirt and bugs can prematurely transition the flow [4]. Moreover, NLF is significantly limited by the wing sweep due to cross-flow instabilities (CF) for high-Reynolds number flows as shown in Figure 2. Consequently, NLF is currently limited to flight-test research aircraft and sailplanes that do not feature deicing/anti-icing systems and also fly at a low Reynolds number compared to commercial aircraft, so their surfaces can have high smoothness and maintain the laminar flow for a significant portion of the lifting surface.

On the other hand, present advances in surface manufacturing applicable for NLF have shown that careful surface treatment may enable NLF for commercial aircraft. One of the recent structural configurations proposed by DLR under the Clean Sky 2 NACOR project features a smooth transition between the nose and the wingbox skin [5]. The demonstrator was manufactured, and the skin structure has also been tested for waviness [6]. Figure 3 shows the connection between the wing leading edge part and the wingbox skin. Two components are connected internally, and the gap is carefully filleted with a composite wedge.

The potential application of NLF to commercial aircraft has been studied by various groups around the world. Although for conventional aft-swept wings boundary layer significantly suffers from the cross-flow instability and high Reynolds number, several methods and aerodynamic solutions are aiming to enable the NLF for conventional wings. Another solution proposed by DLR [7] suggests introducing the forward-swept wing to reduce the wing leading edge sweep, which stimulates cross-flow instabilities, and maintains moderate half-chord sweep to have similar compressibility drag to aft-swept wings. Moreover, forward-swept wings have better low-speed flight characteristics due to the root stall. On the other hand, aeroelastic divergence remains the major issue of forward-swept wings. In addition, forward sweep had a lateral destabilizing effect which needs to be treated with

(a) NLF leading edge

(b) NLF leading edge fillet
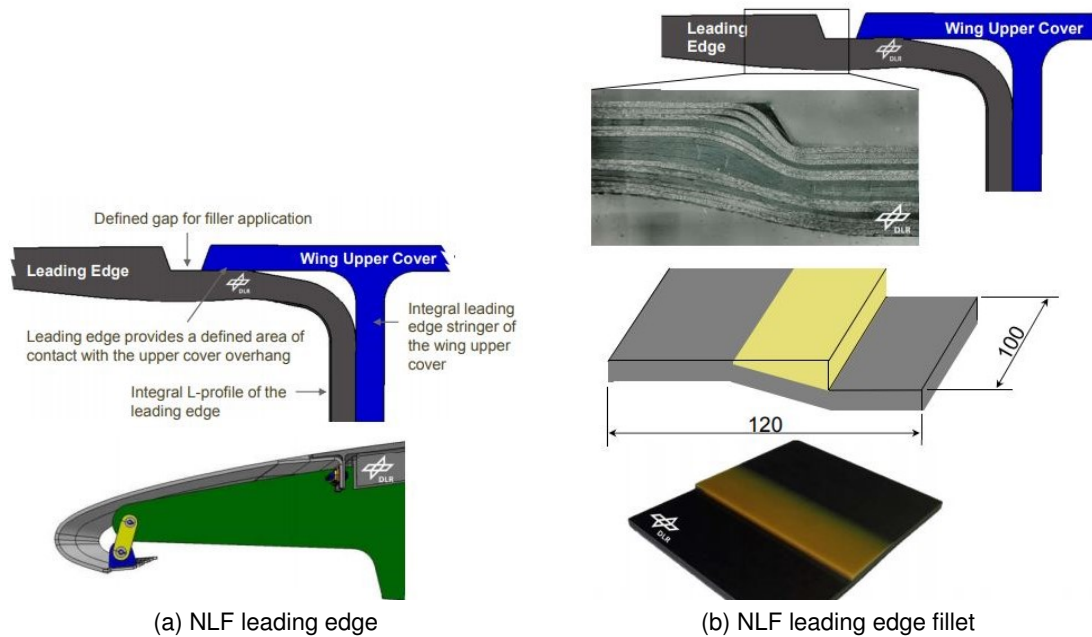
Figure 3 – Composite NLF skin demonstrator concept [5].

care [8]. Recent studies performed by DLR [7, 9, 10] showed the potential of an aeroelastically tailored wing with NLF to improve the fuel efficiency of a short and medium-range aircraft. These outcomes show that despite significant complexities in the design and manufacturing of NLF wings, there is a potential to introduce these technologies into the commercial market. On the other hand, the production and maintenance of such technologies will be complicated for large jets. Additional issues include surface quality maintenance combined with a busy fleet schedule.

Unlike large jets, a typical business jet aircraft have a substantially smaller wing planform, so Re_T can be achieved for a more significant portion of the moderately backward-swept wing (wing sweeps more than $20°$) or can benefit from the forward sweep similar to commercial jets. However, as mentioned before, several uncertainties are present:

1. Is the NLF as an approach for the range extension a significant contributor to the PI as the indicator of the customer interest?

2. How the introduction of NLF technologies may change the aircraft price and if the price can be competitive compared to existing aircraft?

3. What potential aircraft configuration can benefit the most from the NLF introduction?

The present research focuses on the investigation of the potential benefits of the NLF for aircraft in the business jet market and tries to answer the questions stated above. The work is divided into several sections. Section 2 investigates what parameters from the PI definition are more interesting to the customer from the perspective of the aircraft price and if the range extension is a favorable strategy to focus the business jet aircraft design on. Section 3 summarizes Top-Level aircraft Requirements (TLARs) for a selected range of business jets, a light to large jets. Section 4 describes the design methodology and important assumptions. Section 5 describes configurations considered for each business jet category, and Section 6 discusses obtained results.

2. Determination of aircraft price drivers and the design objective

To investigate if the NFL plays an important role in the business jet market, it is first important to know what parameters influence the price the most and what the aircraft price sensitivity to these parameters is. To quantify the customer interest, it can be assumed that the aircraft acquisition price

variation is a measure of customer interest for a given aircraft performance or geometric characteristic. For instance, if the sensitivity of the aircraft price is significantly influenced by the aircraft's maximum range, which in turn can be improved by the introduction of the NLF wing, then the NLF option may have a benefit in the business jet market. On the other hand, if the parameter does not show a significant increase in the aircraft price or other weakly sensitive to the NLF characteristics show substantially more benefit than parameters proportional to the NLF, then the application of the technology will not have potential market benefits.

To determine the aircraft price variation with aircraft characteristics, a model which enables such comparison must be introduced. Various models can be defined based on the importance of certain geometric and performance parameters. The definition used by Isikveren [1] was used in the present research, which defines the aircraft acquisition price based on as

$$Price = f(R_{LRC}, M_{MO}, V_{cab}, S_{cab}, TOFL) \quad (3)$$

where f is an arbitrary function created based on existing aircraft in the market. Here, f depends on the flight range at the long-range cruise speed R_{LRC}, the maximum operating Mach number M_{MO}, the cabin volume V_{cab}, the cabin slenderness S_{cab}, and on the take-off field length $TOFL$. V_{cab} is the cabin volume defined by

$$V_{cab} = \frac{L_{cab}}{4} \left[W_{cab}(\pi H_{cab} + \theta_c W_{cab}) + H_s(2W_{fl} - \pi W_{cab}) \right] \quad (4)$$

In Eq. 4, L_{cab} is the cabin length, W_{cab} is the cabin width, H_{cab} is the cabin height, W_{fl} is the cabin floor width, H_s is the residual vertical height from the maximum width line to the floor defined by

$$H_s = \frac{1}{2} \sqrt{W_{cab}^2 - W_{fl}^2} \quad (5)$$

and θ_c is the angle angle between the maximum width line and the cabin floor defined by

$$\theta_c = \arctan \frac{2H_s}{W_{fl}} \quad (6)$$

Having a sufficient number of airplanes and obtaining their geometric and performance characteristics, a surrogate model of Eq. 3 can be created, which then is used for the sensitivity analysis. To evaluate the price sensitivity to selected aircraft variables, its partial derivatives can be approximated using a finite difference approach evaluated at the price of a given reference aircraft against which the comparison of each aircraft design will be performed.

A set of currently in-service light, mid-size, super-midsize, and large business jets characteristics and their approximate prices have been obtained from online resources. For light jets, the database of airplanes includes Syberjet SJ30i, Embraer Phenom 300, Pilatus PC-24, Cessna Citation Jets 3+ and 4, Learjet 75, and Hawker 400 XP. Mid-size jets are represented by the Embraer Legacy 450 and 500 and Praetor 500, Cessna Citation X, Sovereign, Latitude, and Longitude, and Gulfstream G100. Super mid-size jets include Bombardier Challenger 300 and 350, Gulfstream G250, Embraer Praetor 600, and Dassault Falcon 2000S. Finally, the large jet category includes Bombardier Challenger 650, Gulfstream G350 and 450, Embraer Legacy 600 and 650, and Dassault Falcon 900 LX. A total database of 28 jets was created to build a surrogate model which determined parameters that affect the aircraft acquisition prices in each class. In addition, since the aircraft acquisition price also plays an important role in potential aircraft market applicability, proper price bounds for the future aircraft must be set to determine if the aircraft can be applicable to the given market. Figure 4 shows a chart with acquisition prices of selected aircraft versus the PI. Clouds on the chart represent a typical range of aircraft PI and prices for each business jet market segment. Finally, two solid black lines represent price bounds for future aircraft. Both upper and lower bounds were selected based on the minimum and maximum prices for each category. The linear approximation of the price variation was used similar to Ref. [1]. If the future aircraft does not fit within the boundaries, then its market success most likely is impossible due to an excessive price difference compared to its competitors. From the maximum price standpoint, the aircraft will be too expensive, and its performance benefits may not be worth the money. The minimum price is less strict and indicates an excessively low price for a given
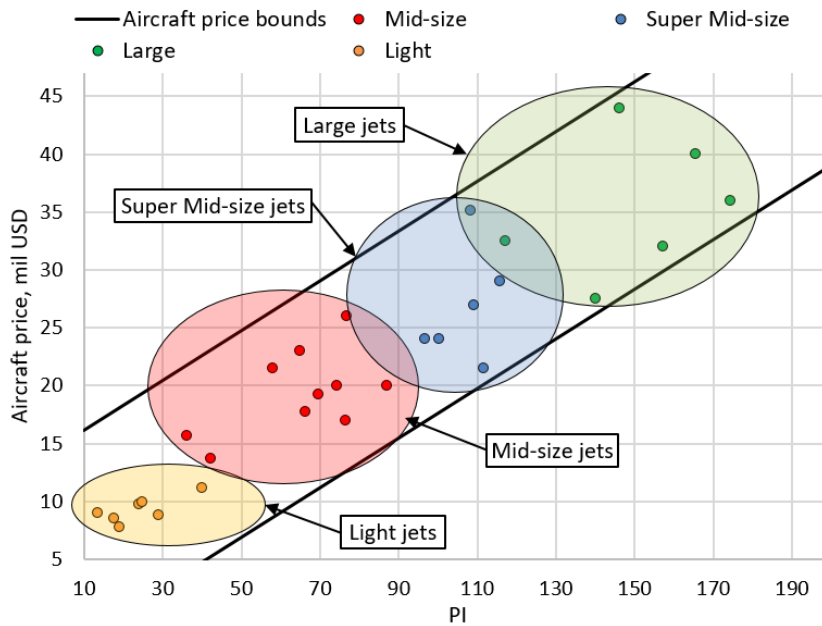
Figure 4 – Productivity Indices versus acquisition prices for light, mid-size, super Mid-size, and large jets.

aircraft. If the minimum price limit for the new aircraft is reached, then it can be easily increased to increase the profit more.

To create a surrogate model based on the existing database, the Regression Learner Toolbox available in MATLAB was used. Out of available regression models, the Gaussian Process Regression algorithm showed the smallest root-mean-square error (RMSE) among other algorithms and was equal to 2.74, which is rather large but is the best accuracy for such a small number of data points. Figure 5 shows a comparison of predicted and actual price values for all selected aircraft. Overall, given a limited amount of aircraft in the database, obtained results show a satisfactory accuracy level.
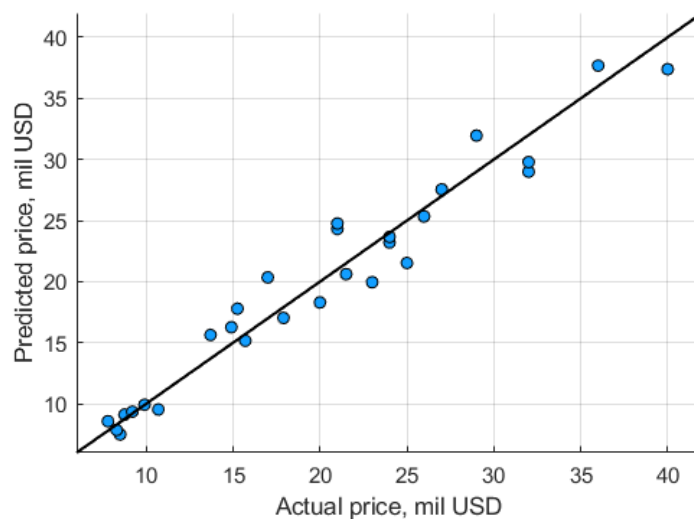
Figure 5 – Comparison of acquisition prices for selected aircraft using the Gaussian Process Regression algorithm.

Having a surrogate model of the acquisition price as a function of aircraft variables, most influential parameters on the aircraft can be obtained. To perform the given task, reference aircraft must be selected. For the light jet category, the Embraer Phenom 300 was selected as the best-selling aircraft in the category. For the Mid-size jet, the Praetor 500 was chosen as the best performing airplane in the class, whose PI is equal to 87. For the Super Mid-size Jet, Praetor 600 was selected. Although

Dassault Falcon 2000S has a slightly larger PI value, Praetor 600 features a significantly longer range and does not have a substantially smaller cabin volume compared to the assault Falcon jet. This combination of aircraft characteristics gives the Praetor 600 the value of 114.4, which brings it to second place among Super-mid size aircraft and is almost similar to the Dassault Falcon 2000S. For the large jet, the Embraer Legacy 650 was selected. Although its PI is the third in the class after Gulfstream G350 and almost similar to G450, its price is substantially lower than G450, and it also features a longer fuselage which is easier to use for investigation of different wing configurations, as will be discussed later.

The goal of the sensitivity analysis is related to an investigation of the average market price trends depending on the aircraft's geometric and performance characteristics. On the other hand, partial derivatives may significantly depend on the point within the surrogate model, so the overall market image is not well-observed. To observe a general market trend, average partial derivatives for each market segment from light to large jets were taken. The average partial derivative is defined by

$$\overline{\frac{\partial Price}{\partial x}} = \frac{\sum_{i=1}^{N} \frac{\partial Price_i}{\partial x}}{\sum_{i=1}^{N} i} \tag{7}$$

where x is the aircraft characteristic and N is the number of aircraft in the database. Assuming that the designed airplane must satisfy the TOFL requirement of a reference aircraft, all remaining variables were changed by 5% with respect to reference values. Figure 6 shows changes in acquisition prices of reference aircraft with respect to the aircraft range at the maximum range cruise speed, maximum Mach number, and fuselage geometric characteristics.

Results demonstrate different trends for each market segment. All market segments demonstrate that the M_{MO} is the most price influential market parameter. However, the difference between the M_{MO} and other parameters vary among segments. The long-range cruise distance R_{LRC} sensitivity has a second place after the M_{MO} for light, mid-size, and super mid-size jets. Moreover, the difference between the M_{MO} and the R_{LRC} reduces with the class. The contribution of the range with respect to other parameters also varies. While cabin dimensions influence is not significantly lower than the range, the difference is more pronounced for mid-size and super mid-size jets. That indicates the priority of the range extension to cabin dimensions for this market segment. For large jets, the cabin length becomes slightly more important than the flight range. The M_{MO} remains the most influential parameter, but its influence is not as significant as for other market segments due to not such a significant variation of M_{MO} for this segment. Based on obtained results, it is observed that the cruise range is generally a major contributor to the aircraft price, although its contribution magnitude varies with the market category. Consequently, it is worth considering the potential benefits of NLF as a range extender for all categories. Although it is expected that the most benefit will be achieved by the mid-size jets, further design assessment will be carried for all studied segments for a complete picture.

The design assessment will focus on the initial sizing of several business jet configurations for each market segment with an objective to maximize the aircraft range with similar Direct Operating Costs (DOC) per year. For each market segment, several configurations will be considered to investigate their range extension potentials, ranges of PI, and aircraft price applicability. The outcome will conclude how much NLF design concepts can extend their range with respect to reference aircraft, how much their productivity is increased, if NLF can be price-feasible for given price constraints, and what configurations will have the best price-productivity combinations for each market segment.

3. Aircraft Top-level Requirements and configurations to consider

Top-level requirements (TLR's) for four business jets are summarized in Table 1 and are based on selected reference aircraft used for the price sensitivity analysis: Embraer Phenom 300, Praetor 500, Praetor 600, and Legacy 650. As mentioned earlier, the design will focus on maximizing the aircraft range without changes in DOC. Cabin dimensions will remain constant for all aircraft to offer similar cabin characteristics to reference aircraft. The mission profile includes the main mission, a 200 nmi reserve, and a 30 min hold at 450 m [11].
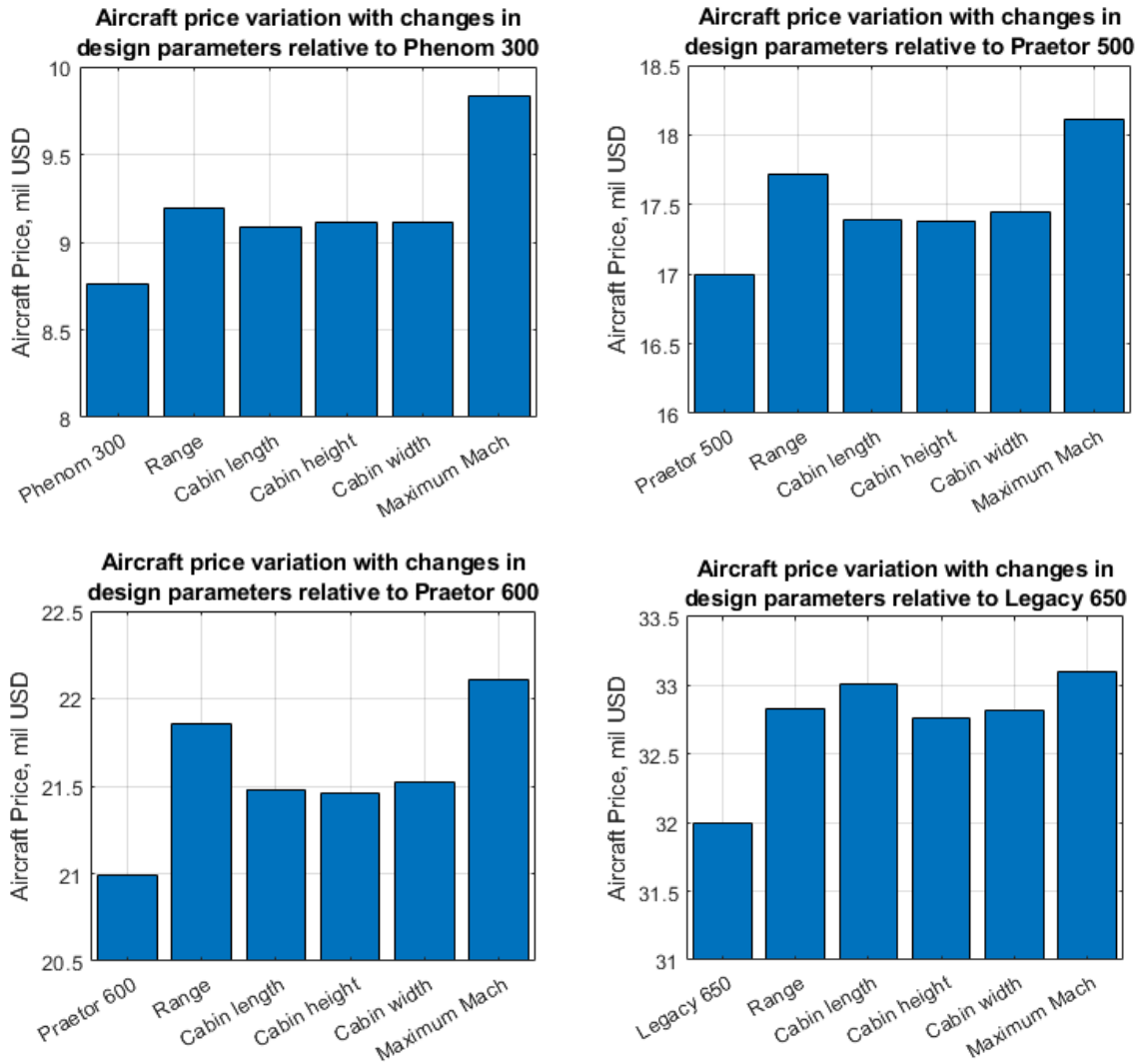
Figure 6 – Aircraft price sensitivity of four reference aircraft with respect to design characteristics.
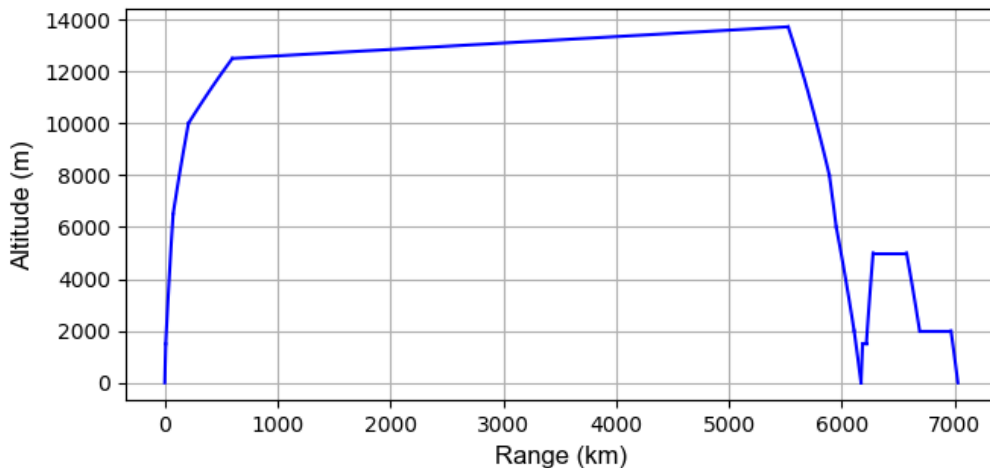
Figure 7 – Designed mission profile.

Several configurations have been selected for the initial sizing to observe the potential influences of different configurations with NLF wings on the market accessibility. Table 2 presents potential configurations for each category. For the light jet, The classical backward-swept wing with fuselage-mounted engines and forward-swept wing with wing-mounted top engines similar to the HondaJet

Table 1 – Top-level requirements for business jets of four different categories.

Parameter	Light	Mid-size	Super Mid-size	Large	Units
Maximum passengers	6	9	12	14	-
M_{LRC}	0.76	0.78	0.78	0.78	-
M_{MO}	0.80	0.83	0.83	0.80	-
Service ceiling	13716	13716	13716	12500	m
Take-off field length	978	1287	1352	1750	m
Landing distance	674	636	692	866	m
Certification			CS-25 [12]		

Table 2 – Aircraft configurations considered for the initial business jet sizing

Light	Mid-size / Super mid-size	Large
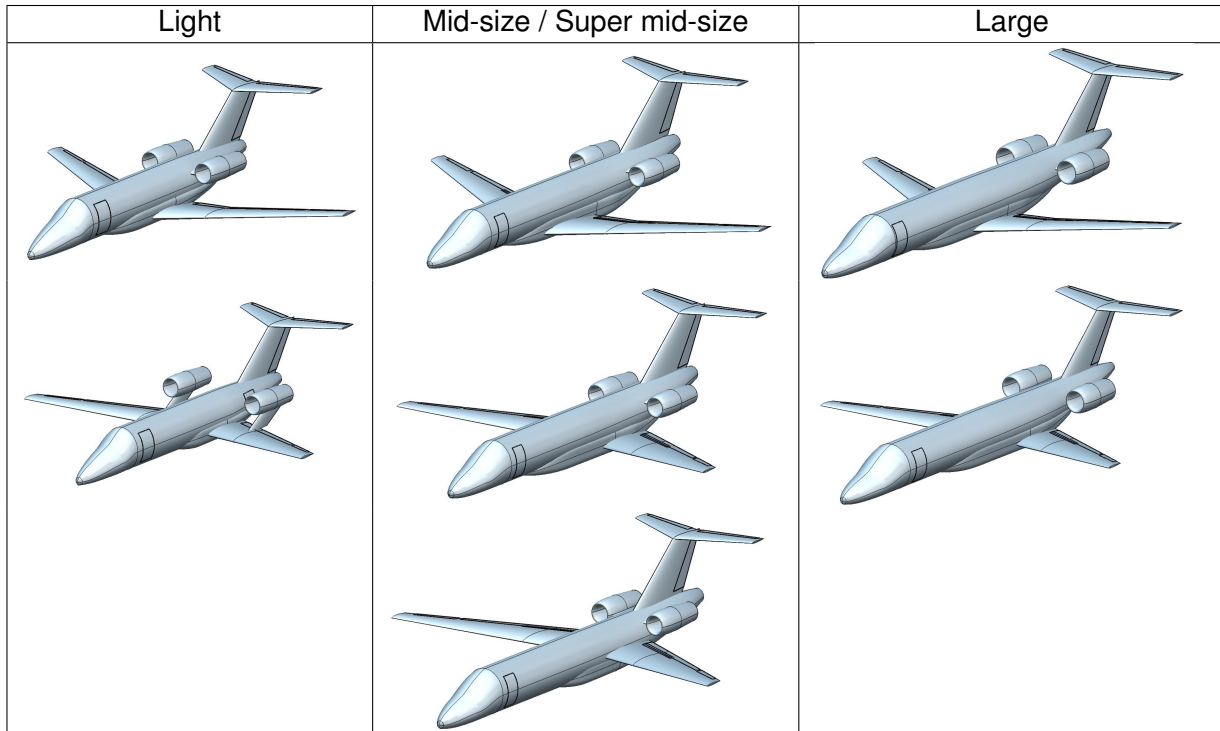
[13] were selected. For the wing-mounted engine configuration, it is assumed that the aft fuselage space where fuselage-mounted engines are generally located is used for the baggage compartment while the wing is located slightly higher than the conventional low wing and the main spar is located aft of the pressure bulkhead. For both mid-size and super mid-size jets, three configurations are considered: the conventional backward-swept wing with fuselage mounted engines, a low-mounted forward-swept wing with fuselage-mounted engines, and the configurations similar to the second one, but with the mid-wing arrangement to reduce the fuselage maximum cross-sectional area. A substantially smaller belly fairing is devoted for a small fuel tank and the landing gear, while most of the fuel is located in the wing and the aft section aft of the pressure bulkhead. The configuration, however, will have a smaller baggage compartment which will be measured and considered during the trade study. Finally, for the large jet, locating the wing aft of the pressure bulkhead is substantially more difficult due to a long cabin. Consequently, two configurations with low-mounted backward- and forward-swept wings are considered.

4. Design methodology and assumptions

4.1 Initial aircraft sizing

The conceptual design was performed using various tools. OpenVSP [14] was used for the aircraft geometric modeling, allocation of critical systems, and their mutual arrangements. SUAVE [15] was used for the aircraft sizing, performance, and mission analysis. The initial sizing within SUAVE fea-

tures constraint diagram initialization using methods described by Gudmundsson [16], the mission simulation, and classical performance analysis routines described in Ref [17, 16, 18, 19].
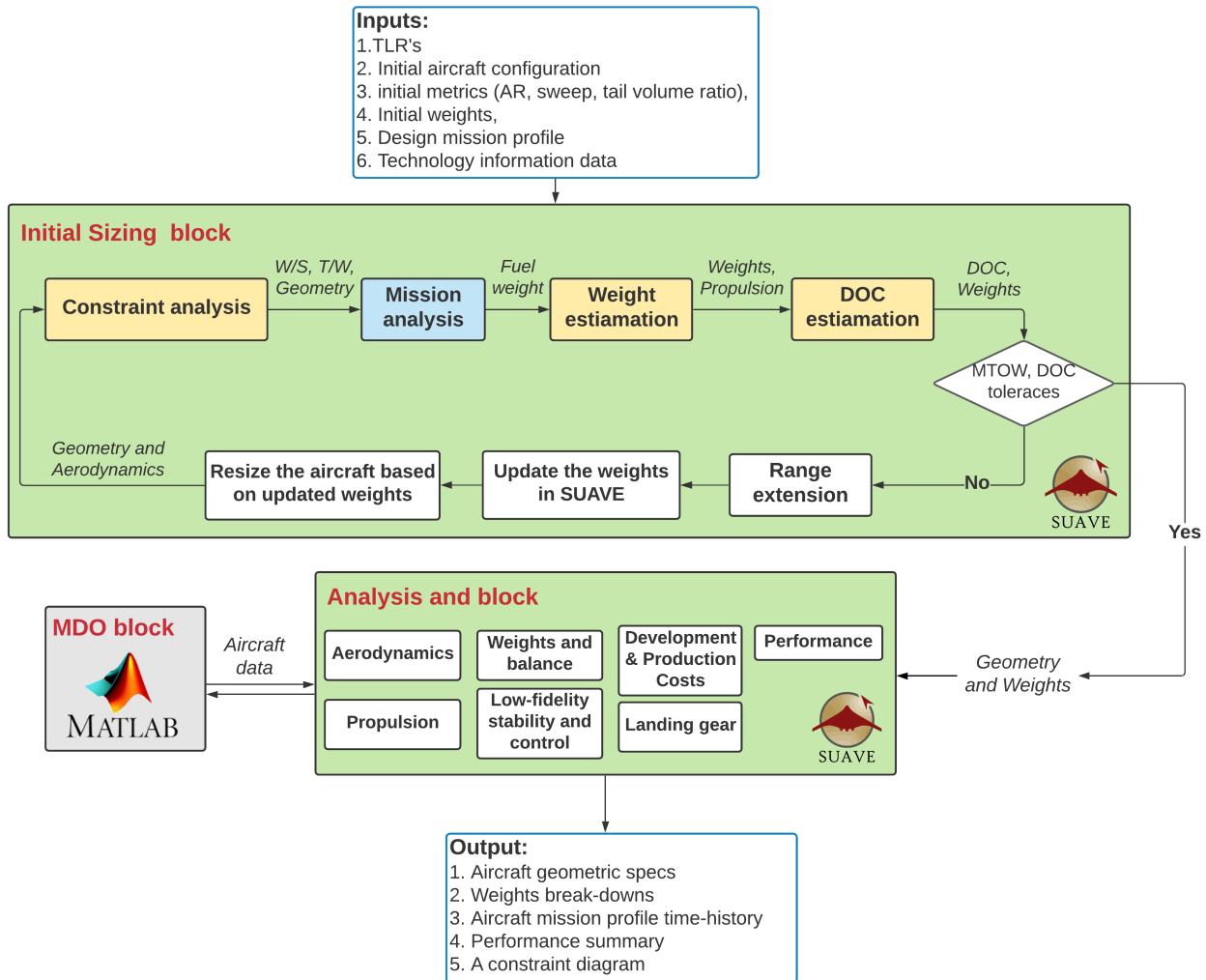
Figure 8 – Initial aircraft sizing framework using SUAVE.

The initial aircraft sizing within SUAVE is performed iteratively, as shown in Figure 8. First, geometric specifications such as the wing aspect and taper ratios, sweep, airfoils, high-lift devices, propulsion system, and tail volume ratios, and initial guessed weights are initialized. In addition, a set of Top-level Requirements (TLR's) and a sample mission profile are initialized. Next, SUAVE performs the constraint analysis to select the first combination of thrust-to-weight ratio (T/W) and wing loading (W/S). Two selection criteria are possible: minimum T/W and maximum W/S. Selected wing loading and thrust-to-weight ratio are used to run the SUAVE mission analyses to estimate the aircraft performance and its required fuel weight which is then used to estimate the aircraft Maximum take-off mass (MTOM). Obtained weights and propulsion system characteristics are used to calculate DOC using the method presented in Ref [20]. Obtained total DOC for a user-defined number of flight hours per year is compared against the reference aircraft DOC obtained using SUAVE. Similarly, MTOM is compared against the value at the previous iteration and is updated if the tolerance is not reached. After the tolerance check, a relative change in yearly DOC per cruise distance is calculated to calculate the new cruise flight range to match the reference DOC. Finally, the next iteration is performed using updated aircraft geometric and propulsion characteristics. Parameters such as the minimum drag coefficient (C_{Dmin}), Oswald efficiency (e), and maximum lift coefficient (C_{Lmax}) for clean and flapped configurations are input into the constraint diagram again to update all constraint curves and runs the next iteration. The solution is terminated when the change in the aircraft MTOM and the difference between the designed and the reference aircraft DOC are reached.

After the initial sizing using the constraint analysis is finished, the program moves to the aircraft performance block to obtain important performance data for the given aircraft. Methods of Torenbeek [18] and Roskam [19] are used within SUAVE to analyze various types of leading- and trailing-edge devices. The empennage sizing within SUAVE is based on the fixed tail volume ratio based on existing reference aircraft. In addition, aspect and taper ratio and sweep are kept similar to reference aircraft to be able to size the remaining geometric parameters. Performance analyses scripts within SUAVE included take-off, all engines operative (AEO), and one engine inoperative (OEI) climb, cruise, descent, and landing.

Finally, an additional refinement using a low-fidelity multi-disciplinary design optimization (MDO) is performed. The objective of the present problem is to maximize the flight range similar to reference aircraft DOC by varying the wing geometry and the engine thrust-to-weight ratio. Constraints for the optimization problem correspond to aircraft performance characteristics defined in the TLRs, performance requirements prescribed by the constraint analysis, a wingtip geometric constraint to ensure manufacturability of the wing, and the wing minimum allowable fuel volume to ensure sufficient overall fuel volume and adequate fuel distribution which will ensure satisfactory aircraft balancing. Table 3 describes the formulation of the optimization problem. There, C_r and C_t are the wing root and tip chords, respectively, t/c is the wing thickness, Λ_{LE} is the wing leading edge sweep, V_{fuel} is the fuel volume within the wing, $V_{fuel,ref}$ is the wing fuel volume of the reference aircraft, and $\eta_{maxcruise}$ is the maximum throttle during the flight at the maximum cruise speed.

Table 3 – Optimization problem definition for mid-size, super mid-size, and large business jets. Values in parentheses indicate bounds for backward-swept wing configurations.

		Lower	**Upper**	**Units**
maximize	Range			
wrt	AR	7.00	11.00	
	λ	0.25 (0.3)	0.45	
	C_r	2.00	4.00	m
	$t/c\|_{root}$	11.00	14.00	%
	$t/c\|_{tip}$	9.00	12.00	%
	T/W	2.5	4.5	N/kg
	Λ_{LE}	-20.0 (15.0)	-15.0 (30.0)	deg
subject to	Take-off field length (TOFL)		TLR TOFL	m
	$T/W - T/W\|_{cruise}$	0.0		
	Landing field length (LFL)		TLR LFL	m
	$\eta_{maxcruise}$		1.0	
	C_t		1.0	m
	V_{fuel}		$V_{fuel,ref}$	m
	$DOC - DOC_{ref}$	0.0	0.0	USD/year

For the MDO, the leading edge sweep angle and taper ratio were limited using several initial considerations. For backward-swept wings, to avoid excessive tip loading, both wing taper and wing sweep were limited to 0.3 and 30 20° respectively. For forward-swept wings, the taper ratio as a contributor to the tip loading is not as critical as for backward-swept wings due to the root-dominant lift distribution. However, forward-swept wings have a lateral destabilization effect on the aircraft. According to Scholz, $10°$ sweep achieves approximately as much as $1°$ dihedral. Moreover, typical wing sweeps for an unswept low wing range between $5°$ and $7°$ and between $2°$ and $4°$ for mid wings [21]. Sweeping the wing forward means the wing needs to increase its dihedral to roughly compensate for the destabilizing effect. Using these relations and limiting maximum dihedral to $8°$ for a low wing to avoid excessive dihedral angles that may significantly increase yaw-roll coupling, the maximum forward sweeps angle of $-20°$ was obtained. It is important to note that such assumptions are rather conservative to avoid overly optimistic results and be reasonable. However, depending on final design outcomes, a more detailed stability and control analysis must be performed. Table 4 summarizes wing fuel volumes for reference aircraft estimated with SUAVE.

Table 4 – Reference aircraft wing fuel tanks volumes estimated with SUAVE.

Parameter	Light	Mid-size	Super mid-size	Large	Units
$V_{fuel,ref}$	2.39	4.1	5.0	6.27	m^3

To perform the MDO, SUAVE was coupled with MATLAB, and the Genetic algorithm was used to find optimal solutions. To account for the constraints, the penalty function similar to one defined in Ref [22] was used. The penalty function is defined by

$$f_p = \mu(y - y_c)\left(\frac{y}{y_c}\right)^\gamma \tag{8}$$

where y is the design variable, y_c is the design variable constraint, μ is the unit step function equal to zero for $y \leq y_c$, and $\gamma = 3$. With the introduction of the penalty function, the objective function becomes

$$f = f + \sum_{i=1}^{N} f_p \tag{9}$$

where N is the total number of design variables. Seventy species per generation were set to have sufficient population size without major accuracy losses. Take-off and landing constraints were calculated using physics-based time-dependent performance formulations described by Gudmundsson [16].

4.2 Calibration of FLOPS weight estimation for business jets

To estimate aircraft weights, the FLOPS [23] method was used within SUAVE. One of the major concerns related to weights estimation at the conceptual design stage is related to uncertainties of the model for a given type of airplane. Since aircraft weights play an important role in the estimation of the new aircraft range benefits, empty weight calibration was performed.

The FLOPS model empty weight estimation was calibrated with respect to several aircraft in the database. Fourteen airplanes were used for the empty weight calibration. Each aircraft was sized and simulated in SUAVE to ensure that FLOPS obtained similar weights to the data available for given airplanes. To match the aircraft weights to their references, an empty weight gain ΔW_e was introduced. The weight gain accounts for differences in empty weights between the SUAVE output and actual aircraft empty weight, so the deviation of the original FLOPS is minimized. The corrected empty weight formulation is defined by

$$W_{e,SUAVE} = W_{e,FLOPS} + \Delta W_e \tag{10}$$

Knowing the distribution of the empty weight gain for each aircraft in the database, the weight gain distribution as a function of the empty weight can be obtained. Figure 9 shows a set of ΔW_e for aircraft included in the database and the final weight curve-fit. The fit relation is then used for the aircraft sizing and is added to FLOPS-obtained empty weight.

4.3 Costs estimation

The estimation of aircraft costs is divided into two components. The first type of costs considered in the analysis which determines the aircraft range extension is the Direct Operating Costs (DOC). The method described by Hoelzen [20] and based on the method of Thorbeck [24] is used to assess the DOC, which is defined by

$$DOC_{Total} = DOC_{Energy} + DOC_{Crew} + DOC_{Ma} + DOC_{Cap} + DOC_{Fees} + DOC_{Cleaning} \tag{11}$$

where DOC_{Energy} are costs of energy, DOC_{Crew} are crew costs, DOC_{Ma} are maintenance costs, DOC_{Cap} are capital costs, and DOC_{Fees} are costs of fees. All costs were calculated in 2021 USD. Unlike the original formulation, an additional parameter of $DOC_{Cleaning}$ corresponding to cleaning fees was introduced. Although maintenance of the NLF surface is substantially less complicated compared to large commercial jets, the importance of additional costs treatment remains.
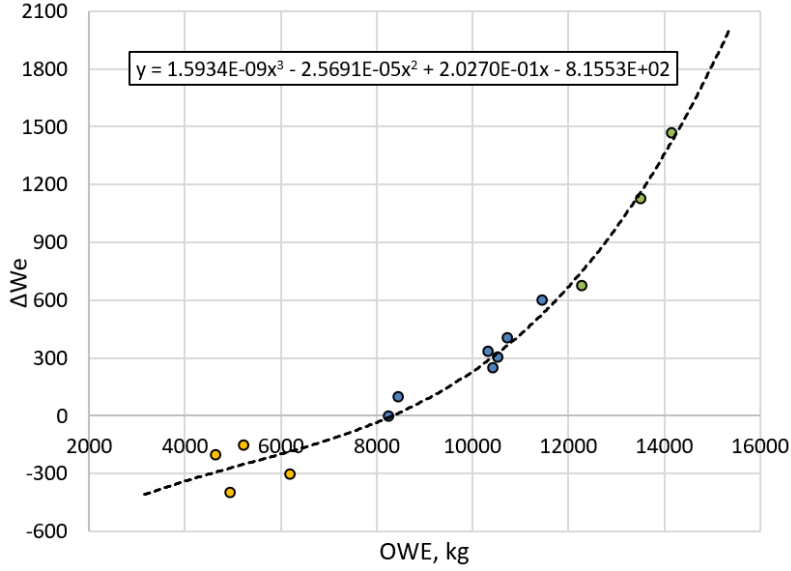
Figure 9 – Empty weight gain factor as a function of the empty weight.

The cleaning DOC estimate is based on the NLF surface area required for cleaning. Based on the Airbus review on aircraft deterioration [25], the approximate time to clean a 0.3 mm roughness height over 1 m^2 takes three man-hours if one person is working. If converted in the rate of cleaning, 100 μm per hour per m^2 is the cleaning speed. The size of dust may range from 1 to 100 μ m, where 50 μm is the minimum object size visible for the human eye. The most important area of cleaning is the wing leading edge of the first 10-15% of the wing. if the dust or contamination average thickness is assumed, then the cleaning DOC becomes

$$DOC_{Cleaning} = \frac{t_{cont}}{R_{clean}} S_{clean} FC \cdot LR \tag{12}$$

where t_{cont} is the average dust or contamination thickness, R_{clean} is the cleaning rate in μm per hour per m^2, S_{clean} is the surface area required for cleaning which can be expressed as a function of the wing wetted area, FC is the number of flight cycles, and LR is the labor rate in USD/hr. For example, if the wing planform with the area of 20 m^2 has a 25 μm (generally, the wing is relatively clean if washed continuously, so a low uniform contamination value is likely) of uniform contamination over the complete leading edge, the aircraft has 400 flights per year, and the labor costs 71 USD/hr, the cleaning will cost 31800 USD/year which is a minor contributor to total DOC which is in the order of millions.

Given methods for DOC estimation are based on conventional metallic aircraft. However, the maintenance cost of composite aircraft parts may vary from metallic parts significantly. Consequently, modifications to maintenance costs are required to account for aircraft composite materials maintenance. The maintenance part of DOC is defined by

$$DOC_{Ma} = (DOC_{AF,mat} + DOC_{AF,per} + DOC_{Eng}) FC \tag{13}$$

where $DOC_{AF,mat}$ are material costs, $DOC_{AF,per}$ are labor costs, DOC_{Eng} are engine costs. For the present research, due to the lack of detailed information and rapid methods to compare maintenance labor on metallic and composite parts, the labor costs are assumed independent of the material used. The material part of maintenance costs is defined by

$$DOC_{AF,mat} = W_{AF}(0.0010136 t_{total} + 0.0012632) + k_{Rep} \tag{14}$$

where t_{total} is the flight time in hours, and k_{Rep} is the repair cost per flight. the airframe weight W_{AF} is defined by

$$W_{AF} = W_{OEW} - W_{Prop} \tag{15}$$

13

where W_{OEW} is the aircraft operating empty weight and W_{Prop} is the propulsion system weight. To account for price differences between metallic and composite materials, a correction factor to material costs must be introduced. As shown in Eq 15, DOC of material is directly proportional to the airframe weight. The airframe weight can be split into components such as the wing, the fuselage, the empennage, and aircraft systems. Each component can have a gain factor that corresponds to the DOC increase due to the use of more expensive materials, so the new material DOC becomes

$$DOC_{AF,mat,new} = DOC_{AF,mat} \sum_{i=1}^{M} \left(\frac{C_i W_i}{W_{AF}} \right) \tag{16}$$

where C_i is the material cost gain equivalent to the ratio between the new material price to the price of the reference material, W_i is the weight of each major aircraft component, and M is the number of airframe components. From Eq. 16, changes in material DOC is directly proportional to the weight of each airframe component and the material cost gain. Knowing what components are designed using specific materials, one can estimate a potential change in overall DOC. For all aircraft components except for the wing, conventional materials are used, so values of C_i are equal to one. For the wing, it is assumed that carbon fiber reinforced plastics (CFRP) are used, so complex shapes such as the upper skin with the front spar can be manufactured and have high smoothness. The main concern is related to the value of C_i for such materials. The only reference presented by Dutton [26] suggests that the ratio between aluminum and CFRP row material costs is equal to 16.0 while finished material costs (for instance, manufactured parts such as ribs) have a ratio of 3.4 due to a large amount of waste during aluminum components machining. For maintenance, both raw materials for patches or local repairs and replacement of components may happen. Consequently, an average value equal to 10 was used for the cost gain due to the implementation of CFRP. Table 5 summarizes important DOC assumptions for the present work.

Table 5 – DOC assumptions.

Parameter	Value	Reference
Fuel rate	5.00 USD/gal	[27]
Labor cost rate	70.8 USD/hr	[24]
CFRP cost gain	10.0	[26]
Crew rate	70800 USD/year	[24]
Pilot rate	177000 USD/year	[24]
Navigation fees	82.6 USD/year	[24]
Depreciation	14 years	[24]

To compare reference and designed aircraft, a fixed number of flight hours per year must be selected for both aircraft. Based on Ref [**?**], an Embraer mid-size jet such as the Legacy 500 flies for more than 700 hours per year if operated by charter operators, while single aircraft operators typically fly theirs 150–200 hours per year. To account for both operation types, an average value of 450 hours per year was chosen for all benchmark and designed aircraft DOC estimations.

Validation of the DOC model was performed with respect to values estimated by the 'Compare Private Planes' resource [28] where the cost break-down is estimated using an in-build cost estimation model. Figure 10 compares results obtained using both methods for sixteen aircraft for 450 flight hours per year. Results demonstrate higher DOC for the SUAVE-embedded model compared to the reference resource for nearly all aircraft. Six aircraft demonstrate DOC differences of between 10% and 15% while other aircraft have errors not exceeding 8% with the majority having values of 5% and less. The average error for the complete set is equal to 7.4%. Due to complexities in DOC estimations and variations of models, differences are expected, but the general trend allows the model to be used for the analysis knowing that the 95% confidence level ranges between 5.13% and 9.7%.

The second type of cost used for the design assessment is the development and acquisition cost. The assessment of these costs determines if the aircraft price may be applicable to the market even though DOC benefits may be present. To ensure a potentially successful demand of the aircraft on
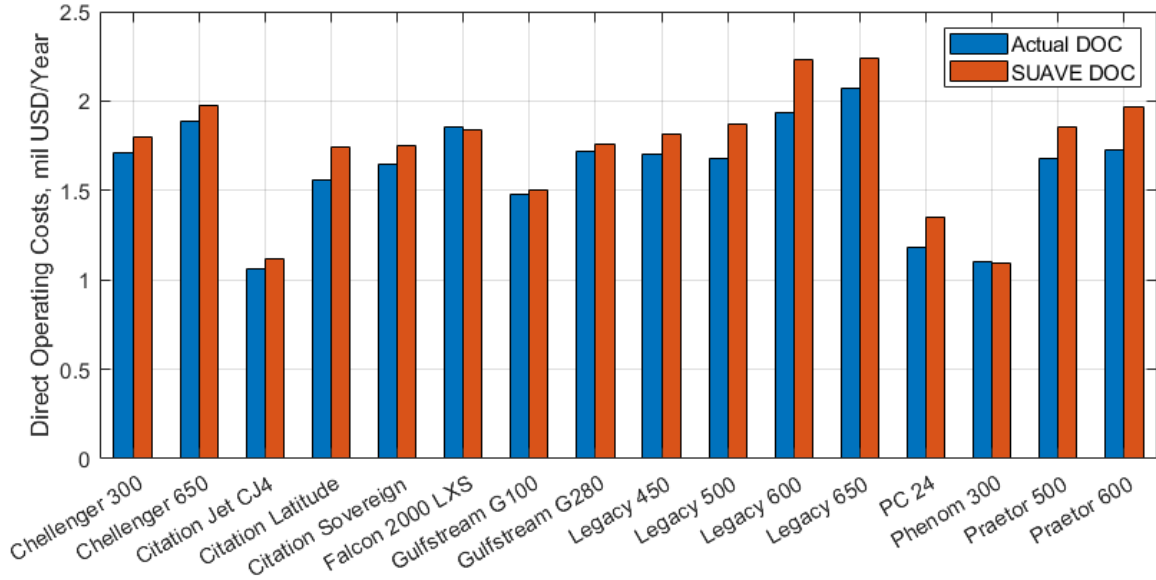
Figure 10 – Comparison between SUAVE-estimated aircraft DOC and DOC from the database for reference aircraft.

the market, its development costs shall fit within the bounds of initially determined prices shown in Figure 4. Preferably, the aircraft price shall not significantly exceed the price of the reference aircraft to be more advantageous for the potential customer. Aircraft development costs were estimated using the method provided by Roskam[19]. Development and acquisition costs are divided into multiple components. Development costs are defined by

$$C_{RDTE} = C_{aed_r} + C_{dst_r} + C_{fta_r} + C_{fto_r} + C_{tsf_r} + C_{pro_r} + C_{fin_r} \qquad (17)$$

where C_{aed_r} are airframe engineering and design costs, C_{dst_r} are development support and testing costs, C_{fta_r} are costs related to the manufacturing of flight test prototypes, C_{fto_r} are flight test operations costs, C_{tsf_r} are test and simulation facilities costs, C_{pro_r} is the profit embedded into the program, and C_{fin_r} are costs of financing.

Acquisition costs are defined by

$$C_{ACQ} = C_{MAN} + C_{pro_m} = C_{aed_m} + C_{apc_m} + C_{fto_m} + +C_{fin_m} + C_{pro_m} \qquad (18)$$

where manufacturing costs C_{MAN} are split into airframe engineering and design costs for manufacturing C_{aed_m}, airplane program production costs C_{apc_m}, production flight test operations costs C_{fto_m}, costs of financing during the manufacturing phase C_{fin_m}, and the embedded profit C_{pro_m}.

Multiple costs assumption has been made to designed aircraft configurations. For all aircraft, the value C_{pro_m} was assumed 10% of final total costs, and C_{fin_m} also assumed 10% of total costs, similar to recommendations of Roskam. To account effects of advanced technologies, the method of Roskam uses factors to estimate costs gains due to various material types and aircraft development complexity within the model. For moderately advanced technologies, Roskam recommends the factor of 1.5, while for aggressively advanced, the factor of 2.0 is recommended. Two aspects of NLF aircraft create major design complexities. First, manufacturing of the NLF structure and satisfaction of necessary tolerances. Second, aircraft that feature a forward-swept wing of wing-mounter over-the-wing engines will further increase the complexity. If the aircraft features a backward-swept wing, most additional complexities are related to the design and manufacturing of the NLF composite wing, which is a moderately complex task, so the factor between 1.4 and 1.6 is used. The range of factors is used to capture sensitivities of costs to technology assumptions. If the wing is forward-swept and is mid-mounted, then the wing needs to be carefully tailored to avoid substantial weight penalties due to aeroelastic divergence. Moreover, the destabilizing nature of the forward-swept wing needs to be treated carefully by the airframe design and additional control system capabilities. Since the design

complexity increases, it is assumed that factors between 1.5 and 1.7 are used. If the wing is forward-swept low-mounted wings, the destabilizing effects are stronger than for the mid-mounted ones, so all gains were assumed 0.05 larger than for mid-mounted wings. Finally, if over-the-wing mounted engines similar to HondaJet are used. An additional gain of 0.05 is assumed. Table 6 summarizes possible combination of complexity assumptions. For the material gain factor, only the wing features composite materials. According to Roskam, the gain factor for composite materials for the complete aircraft range from 2.0 to 3.0. The amount of composite material used for the wing can be crudely approximated by the wetter area ratio between the wing and the complete aircraft. For business jets in the database, the ratio of wing wetter area to the total wetted area is approximately 0.33. The material factor gain then cab be approximated as a linear function of the wetted area ratio

$$F_{mat} = k \left(\frac{S_{wet_{wing}}}{S_{wet_{total}}} \right) + m \tag{19}$$

where coefficients k and m are found using appropriate material cost gains boundary conditions. For the present study, the boundary conditions are

$$F_{mat} = \begin{cases} 1, & \left(\frac{S_{wet_{wing}}}{S_{wet_{total}}} \right) = 0, \\ F_{mat_{max}}, & \left(\frac{S_{wet_{wing}}}{S_{wet_{total}}} \right) = 1, \end{cases} \tag{20}$$

where $F_{mat_{max}}$ is the maximum possible material cost gain factor (as mentioned earlier, the factor ranges from 2.0 to 3.0). Solving Eq. 20, the material gain factor between 1.33 and 1.66 is obtained.

Table 6 – Complexity gain factors for development costs.

Technology combination	Factor range
BWD-swept composite low-wing	1.40 - 1.60
FWD-swept composite mid-wing	1.50 - 1.70
FWD-swept composite low-wing	1.55 - 1.75
FWD-swept composite low-wing + over-the-wing engines	1.60 - 1.80

Finally, the aircraft unit price to be compared against reference aircraft in the market is defined by

$$P_{unit} = \frac{C_{RDTE} + C_{ACQ}}{N_{prog}} \tag{21}$$

where N_{prog} is the expected number of aircraft developed during the program. Existing information about annual sales for various business jet models was obtained from Ref. [29] and an average annual sale for each reference aircraft was estimated. In addition, three test aircraft were added during the development program. The production program of ten years was assumed.

To ensure sufficient accuracy of the Roskam's development costs model, several database aircraft prices were estimated and compared against existing database information. Price estimates of selected business jets were obtained from the 'Air.one' online database, which includes either actual jet prices recommended by the manufacturer or the price estimate using internal models [30]. Comparison between SUAVE-modeled prices and reference values are presented in Figure 11. Obtained results demonstrated a satisfactory distribution of errors. A relative error for most aircraft does not exceed 10%. However, four aircraft out of sixteen demonstrated errors between 10% and 15%, and one aircraft had an error of 23%. The average difference between SUAVE and reference absolute prices for all sixteen aircraft is equal to 7.95%. The 95% confidence interval ranges between 5.2% and 10.7%, giving sufficient accuracy for the model.
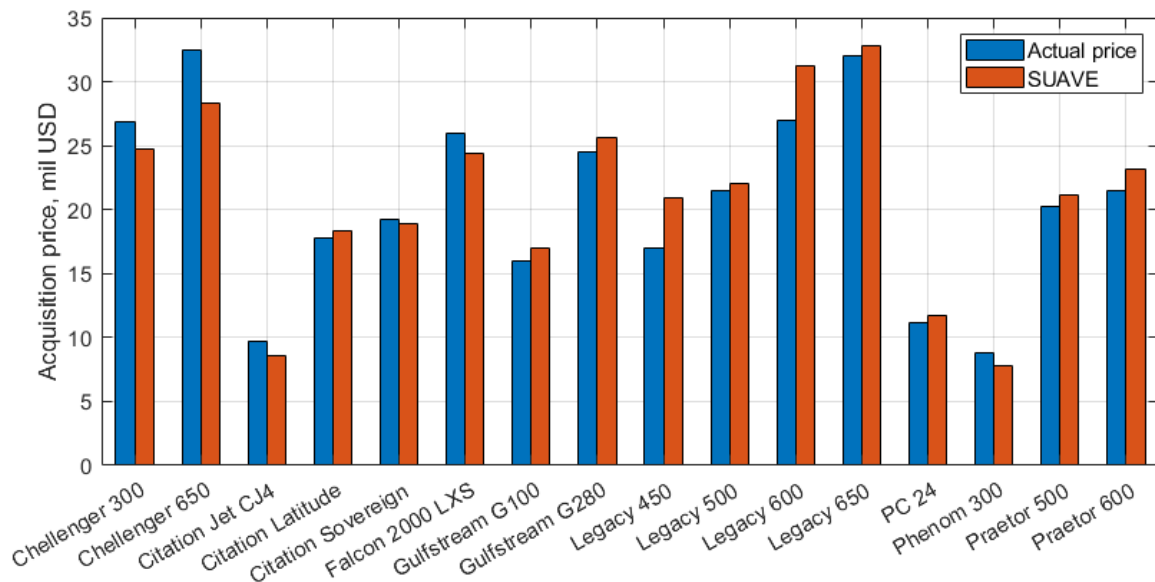
Figure 11 – Comparison between SUAVE-estimated aircraft prices and prices from the database for reference aircraft.

5. Initial aircraft sizing considerations

Multiple aspects of the initial sizing were considered to ensure sufficient accuracy of models representation. For the fuselage, every aircraft features similar cabin dimensions to ensure the equivalent comparison between designed and reference aircraft. Then, depending on the configuration, the remaining aircraft components are located according to the constraint analysis, MDO studies, and weights and balance assessments. Figure 12 demonstrates a sample layout of the mid-size aircraft with a mid-located forward-swept wing where cabin components, areas indicated for fuel, systems, landing gear, and APU are represented. While aircraft with low-mounted wings and fuselage-mounted engines do not represent major changes from the original system's layout inside the fuselage, the mid-wing and aft-mounted engines layout involve additional design assumptions. For the mid-wing, extra fuselage length is required to fit the wing behind the pressure bulkhead. For both mid-size and super mid-size jets, an additional 0.75m was added to the fuselage length to fit the wing. For the light jet with wing-mounted engines, the original fuselage can be reduced since the volume required for the engine pylon becomes free. According to Nicolai [31], a similar configuration of a HondaJet managed to increase the fuselage volume by almost 20%. However, if the wing is swept forward, the wing root is located in the region where the baggage was located for the conventional aft-swept wing configuration. Consequently, the free space can now be used for the baggage compartment. Due to the redistribution of components within the fuselage, no fuselage extension or reduction was assumed. In addition, the wing root can be partially lifted up to reduce the fuselage pressure drag, similar to the mid-wing configuration.

The wing design assumptions play an important role in overall aircraft performance estimation and shall be treated carefully to ensure the capabilities of the wing to be manufactured and maintained. Figure 13 shows a schematic layout of the wingbox and the example upper skin with spars and stringers manufactured during the LOMACHS project [32]. The leading edge skin can be manufactured using carbon fiber reinforced plastics (CFRP) with advanced anti-icing technologies or feature conventional anti-icing systems. The leading edge is mounted to the main wingbox with consists of the integral upper skin and the main spar part, the lower skin, and the rear spar. The lower skin is attached using rivets which makes the wing easier to design and maintain since the lower skin can be unmounted to access the wingbox and work on internal systems. However, the transition of the boundary layer on the pressure side will happen early, so NLF was not considered for the pressure side of the wing. The upper skin and the leading edge are connected using a smooth fillet similar to the one shown in Figure 3, so sufficient smoothness can be achieved, and the NLF can be extended on the suction side for as long as possible. Finally, the leading edge is bolted to the main spar and can
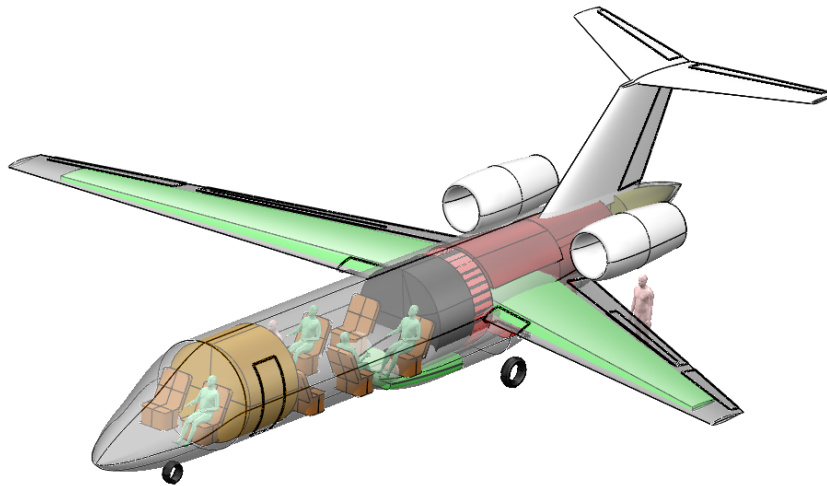
Figure 12 – Geometry of a mid-size jet and its internal layout. Green areas represent fuel tanks, a golden section defines the galley, black segment shows the lavatory, red area defines the systems section, and yellow represents the APU
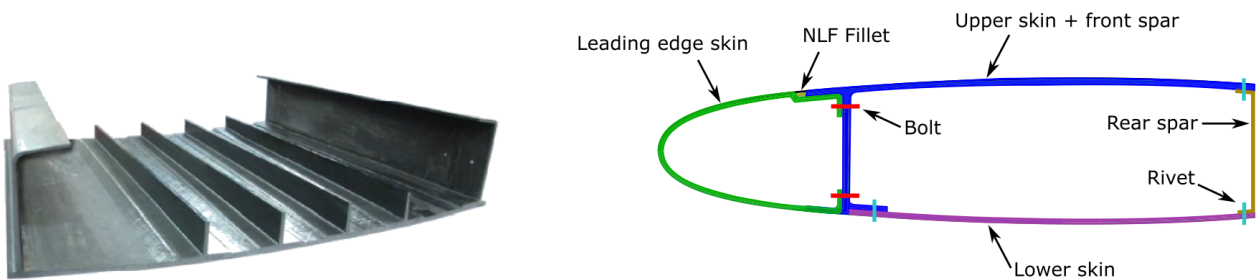
Figure 13 – A schematic structure of the wingbox featuring NLF and a sample manufactured upper skin [32].

be replaced by accessing the wingbox from the pressure side. Doe to the application of composite structures, wing weight assumptions must be implemented. According to Raymer [17], up to 15% of the wing weight with respect to metallic structures can be reduced if advanced composites are implemented. For conventional backward-swept wings, a more conservative assumption of 10% reduction was used. For forward-swept wings, Kruse demonstrated potential reduction of the wing weight by 8% compared to a conventional aluminum wing [33]. To maintain conservatism in the design due to limited research on forward-swept wings weight estimation, an assumption of no weight change of a forward-swept wing with respect to a backward-swept aluminum wing was implemented.

The pressure side transition is assumed at a 10% chord close to the end of the anti-icing system. The transition model for the wing is based on the flight test data of F-14 conducted by NASA [34, 35] where the maximum transition Reynolds number (Re_T) was measured as a function of the wing sweep for the wing root, mid-section, and tip. Plots of Re_T as a function of the wing sweep and Mach number were digitized to obtain a universal curve fit. While Re_T for a given leading-edge sweep demonstrates variations with Mach number, variations are not significant, and average values were obtained for each sweep which is sufficient for the initial design assessment. Although the mid-range aircraft airfoil design performed by Seitz showed the transition location at 60% chord [9], maximum transition location was limited to 50% due to the flight test NLF glove limitation. Such assumption captures the majority of the potential boundary layer and can demonstrate potential NLF benefits, although being potentially conservative. In addition, although the flight test data was used for the boundary layer transition simulation, the boundary layer behavior at various atmospheric conditions is still uncertain. Later design stages shall either implement a more sophisticated surrogate model or include direct airfoils design and the regression model of an actual wing. Figure 14 presents curve fits for the root,
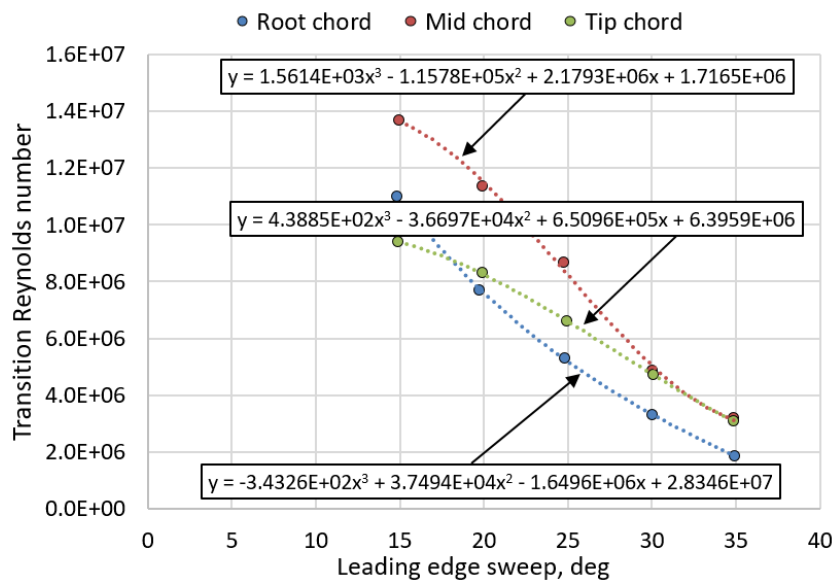
Figure 14 – Transition Reynolds number as a function of the wing leading edge sweep for the wing root, mid-section and tip [34, 35].

mid-, and tip chords as a function of the wing leading edge sweep.

Table 7 – Summary of assumption considered for each designed aircraft.

Aircraft	Wing weight gain	Fuselage extension	Boundary layer transition	Engine interference
Lightjet, BWD-swept wing	-10% wing weight	-	Re_T regression	-
Light jet, FWD-swept wing, wing-mounted engines	-	-	Re_T regression	+0.1 factor
Mid-size jet, BWD-swept wing	-10% wing weight	-	Re_T regression	-
Mid-size jet, FWD-swept wing	-	-	Re_T regression	-
Mid-size jet, FWD-swept mid-wing	-	+0.75 m	10% root chord, regression otherwise	-
Super mid-size jet, BWD-swept wing	-10% wing weight	-	Re_T regression	-
Super mid-size jet, FWD-swept wing	-	-	Re_T regression	-
Super mid-size jet, FWD-swept mid-wing	-	+0.75 m	10% root chord, regression otherwise	-
Large jet, BWD-swept wing	-10% wing weight	-	Re_T regression	-
Large jet, FWD-swept wing	-	-	Re_T regression	-

All aircraft feature single-slotted flaps for low-speed operations, while for the mid-size and super mid-size jets with mid-wings, an inboard droop nose similar to the one used for the HFB 320 Hansa Jet [36] was considered. Since forward-swept wings stall from the root and engines are located almost directly behind the wing (unlike a low wing where a more pronounced clearance exists), a separated

flow may be sucked by the engine and may substantially influence the engine performance. To avoid such a situation, a leading-edge droop nose with the span on the engine diameter is introduced. The transition at the droop nose is assumed similar to the pressure side of the wing and equals 10%. Two regions between the droop nose and the outer wing are separated by the fence to minimize spanwise flow and achieve a more uniform engine inflow profile. Outside of the droop nose, the model similar to other wings is used.

The contribution of wing-mounted engines was assumed to have additional interference drag due to higher speeds experienced by the pylon mounted near the wing. The engine interference factor was increased by 0.1 to account for this potential effect.

Finally, empennage, engine nacelles, and fuselage do not feature NLF, and their transition was assumed 10% for the empennage, 5% for nacelles, and 0% for the fuselage. Table 7 summarizes all critical assumptions considered for all aircraft.

6. Initial sizing results and discussions

Figures 15 and 16 demonstrate the boundary layer transition line estimates for each designed aircraft configuration after their initial sizing and refinements using MDO. For light jets, both transition lines reach a maximum allowable chord ratio of 50% due to relatively low operational Reynolds number. For mid-size and super mid-size jets, aft-swept wings show earlier root transition due to a higher leading-edge sweep and Reynolds number and achievement of 50% laminar boundary layer at the mid-span. Starting from the super mid-size category, forward-swept wings also start demonstrating earlier root transition compared to smaller business jet categories. As discussed before, mid-wing configurations feature a droop nose which limits the root boundary layer to almost fully turbulent.

(a) Light jets boundary layer transition   (b) Large jets boundary layer transition
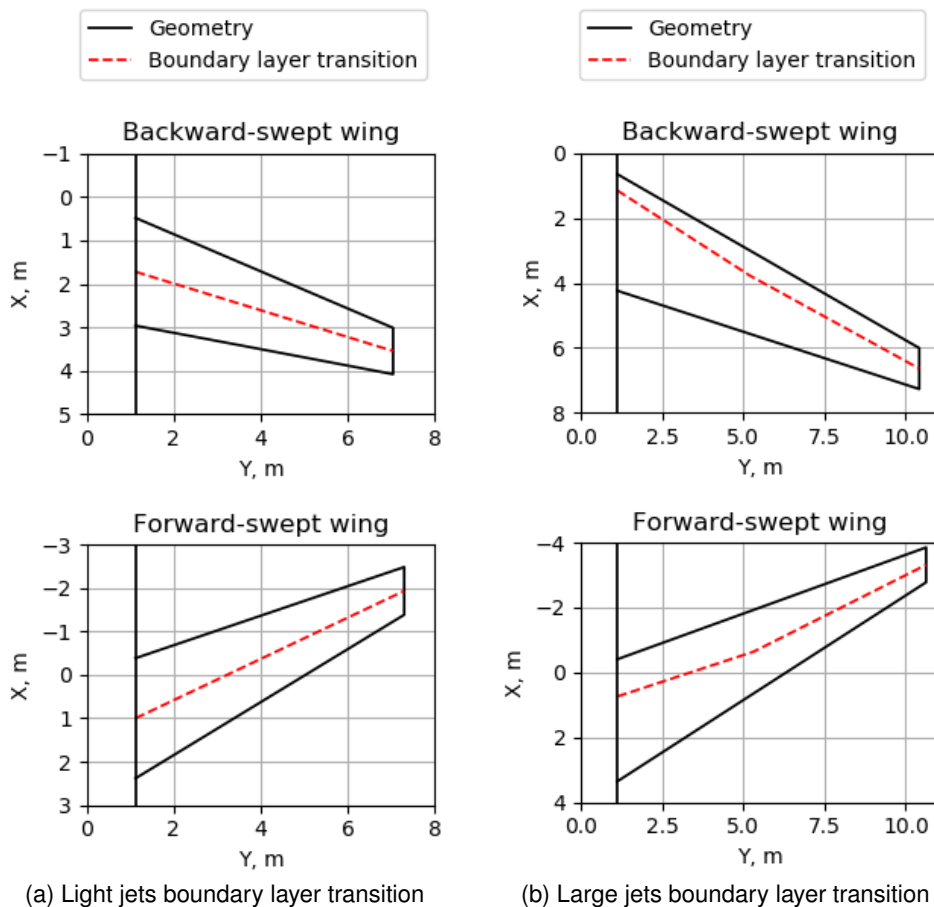
Figure 15 – Boundary layer transition profiles for light and large NLF aircraft.

Tables 8-19 in Appendix summarize sizing and MDO results for each designed aircraft configuration. Several trends can be observed for all configurations. First of all, all forward-swept aircraft configura-

(a) Mid-size jets boundary layer transition

(b) Super mid-size jets boundary layer transition
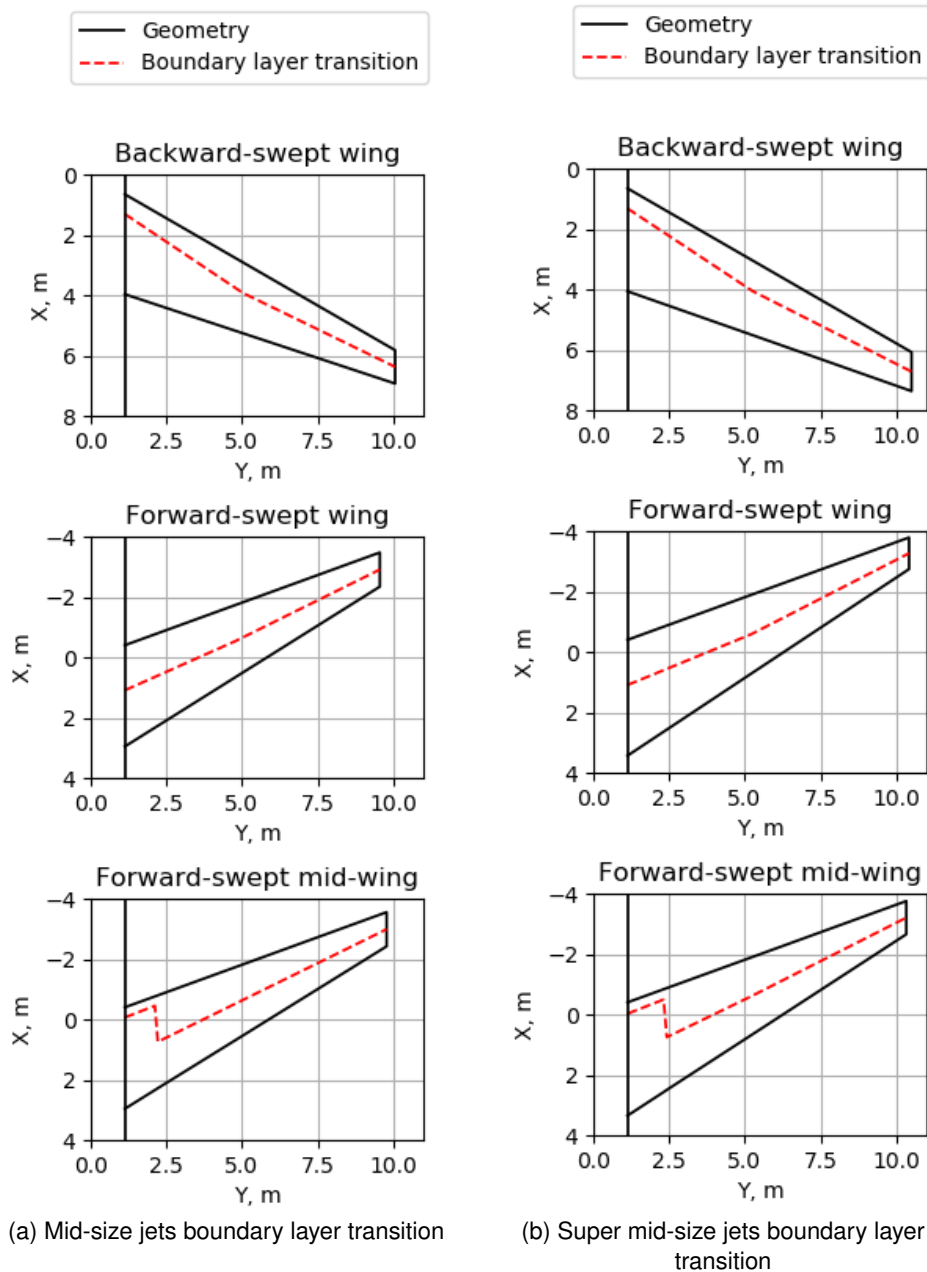
Figure 16 – Boundary layer transition profiles for mid-size and super mid-size NLF aircraft.

tions approach to maximum allowable wing sweep to minimize the compressibility drag. In addition, their aspect ratio also reduces so that a larger mid-chord sweep angle can be reached and the compressibility drag is reduced more. Second, overall thickness for all aircraft approaches minimum values but does not reach minimum values due to both the fuel volume constraints and wing weight penalties due to thickness. As expected, all forward-swept configurations feature slightly larger horizontal and vertical stabilizers due to reduced tail arms and effects of less slender planforms. The weight breakdown of each configuration depends not only on the boundary layer transition profile but also on weight reduction assumptions and additional drag penalties for each configuration. In addition, assumptions affect maximum aircraft ranges for similar values of DOC. The combination of all these considerations results in a unique aircraft ranking with respect to particular parameters. Both forward- and backward-swept light jets can reach nearly similar ranges, while the backward-swept configuration has a superior take-off performance. On the other hand, due to the higher wing loading, its landing distance is larger than the forward-swept one. For mid-size jets, the wing weight reduction and a relatively large percent laminar flow drive the configuration to minimum weights among

other configurations while having the best range. Moreover, low weights also allow slightly better field performance. The mid-wing configuration demonstrates the worst range improvement. Although the fuselage pressure drag was reduced, the droop nose compensated for these benefits and even added more drag. For the super mid-size category, the wing weight penalty did not play a major difference making the backward-swept and forward-swept configurations nearly similar with respect to the range. However, the backward-swept configuration has a superior take-off performance. Finally, for the large category, only a minor difference in range between the aft-swept and forward-swept configurations exist, but the performance differences are minor. On the other hand, the weight benefits of the aft-swept configurations remained.
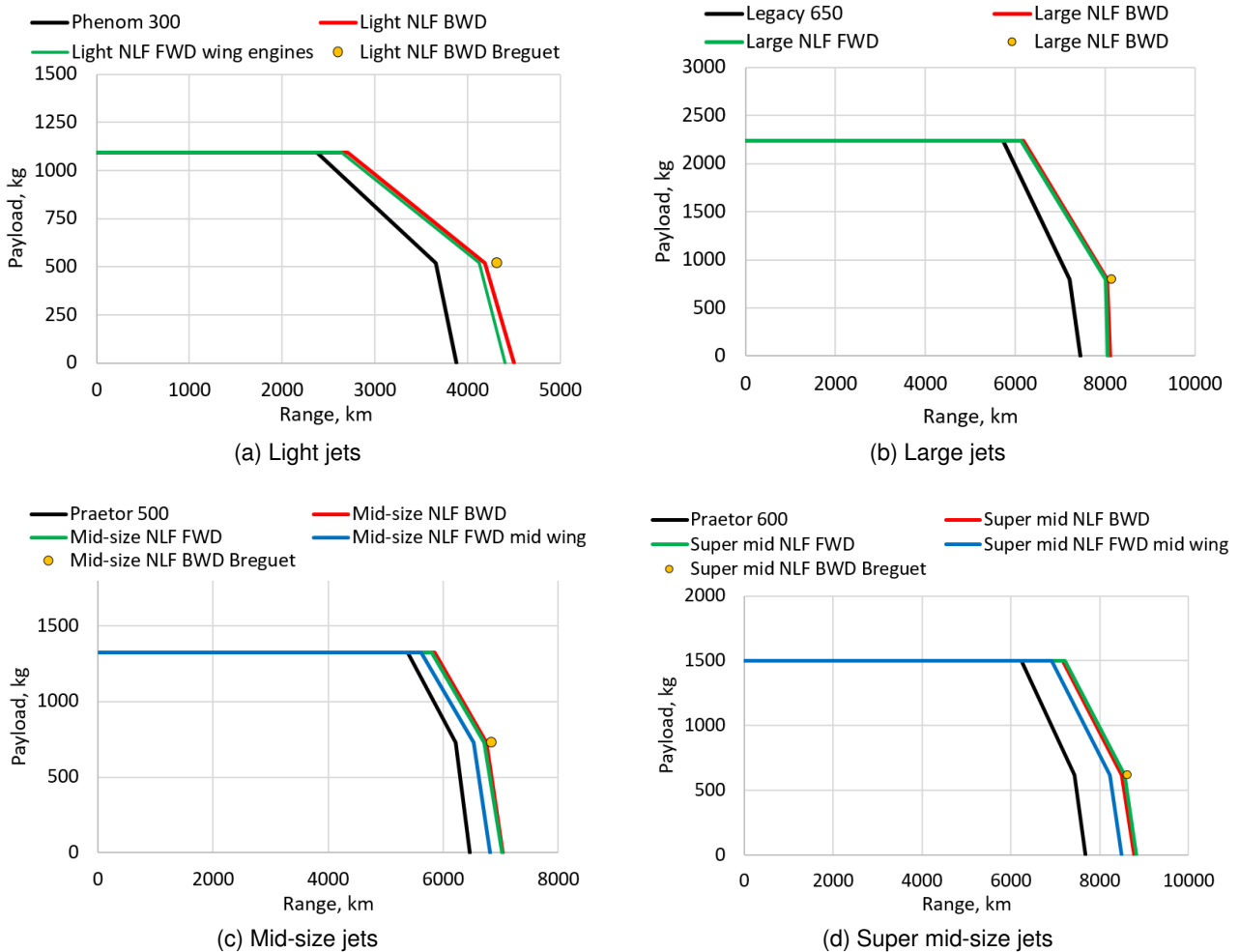
Figure 17 – Payload-range diagrams of designed aircraft.

In general, all aircraft configurations have lower weights compared to reference aircraft, both due to the influence of NLF and technologies required for its implementation. As a consequence, the ranges of all aircraft increased compared to their references. Figure 17 shows payload-range diagrams for all configurations with respect to their references. For additional SUAVE validation, a single point for each backward-swept NLF configuration was compared against the range estimation using the Breguet range equation. Comparison of SUAVE and Breguet range equation results shows acceptable similarity. If all configurations are compared to their references, the flight distance extension with four passengers ranges from 5% to 15% depending on the configuration. The lowest change in range was achieved by the mid-size forward-swept mid-wing jet, while the maximum extension was achieved by the super mid-size forward-swept low wing configuration.

Finally, the aircraft acquisition price for each NLF jet is presented in Figure 18. Colored circles on the PI chart represent initially bounded business jet market areas, and designed aircraft were plotted with existing aircraft to create specific ranges of potential PI indices and prices for each NLF aircraft

group. Moreover, each aircraft price was represented as a range of values depending on technology and material costs assumptions. A more direct assessment of the aircraft price with respect to their reference aircraft and average market values is presented in Figure 19.
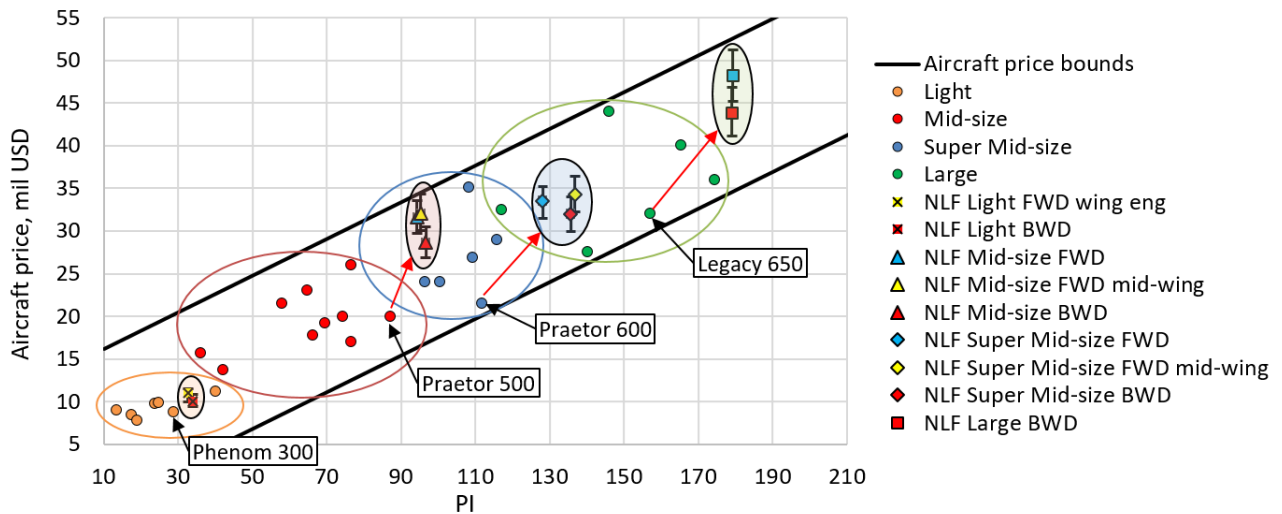
Figure 18 – Productivity Indices versus Prices for designed aircraft.
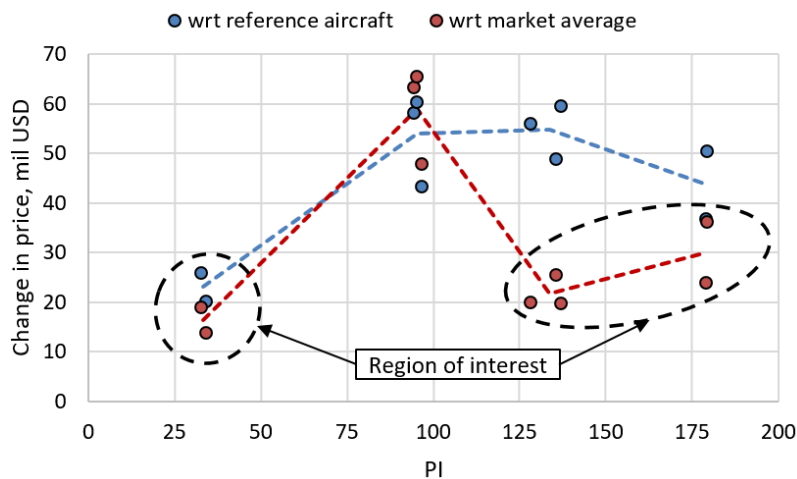
Figure 19 – Comparison of NLF aircraft prices with respect to reference aircraft and market average prices.

For light aircraft, the introduction of NLF leads to a minor increase in aircraft productivity compared to its reference to relatively low overall values of PI indices and lower contribution of the range as the PI index driver compared to other market segments. The price of NLF light jets increased by approximately 20% with respect to both reference and market values and became one of the more expensive jets in the category. However, due to a generally large production volume of aircraft similar to Embraer Phenom 300, production cost gains are redistributed such that the absolute price increase is not substantial. Observing the mid-size category, NLF aircraft demonstrate a significant increase in productivity due to the range extension and its influence on the PI index. Moreover, the increase in range moved the mid-size jet into the super mid-size category with respect to the PI index. However, technology and material cost penalties significantly increase the aircraft prices, moving it to the upper end of price bounds. The backward-swept configuration shows the lowest possible price due to the lower empty weight, which is the major driver of the Roskam development costs model. Forward-swept versions, however, approach the price boundary making these aircraft rather luxurious from the price perspective. The change in price with respect to both the reference and market average values is around 55%. The super mid-size category demonstrates the strongest increase in the PI

index compared to all other segments. In addition, due to the reference configuration with a significant range extension, the NLF configuration also achieved the largest increase in range. Similar to the mid-size category, these aircraft have moved to the large category from the productivity perspective. The price has also increased by 55% with respect to the Praetor 600. However, according to the database, this aircraft has the lowest price in the market. If NLF jets are compared against market-average values, the increase in 20% is observed, making this jet close to the medium price range in the category and potentially interesting for customers due to the maximum range around 8500 km (14% larger than the reference aircraft) and operating costs of the Praetor 600. For large jets, the range extension had a similar impact and magnitude of super mid-size jets. However, since the reference aircraft price is larger, the effect of price gains is stronger. While the backward-swept configuration is located in the middle of the price bounds, the forward-swept configuration demonstrates higher prices with similar performance. The change in price with respect to the reference aircraft is equal to 45% if prices are compared to the market average, the price increases by 24% for the backward-swept. If compared to prices of existing large jets, the backward-swept configuration may make a higher-end model in terms of price offering a 12% range extension at similar operating costs. To fully
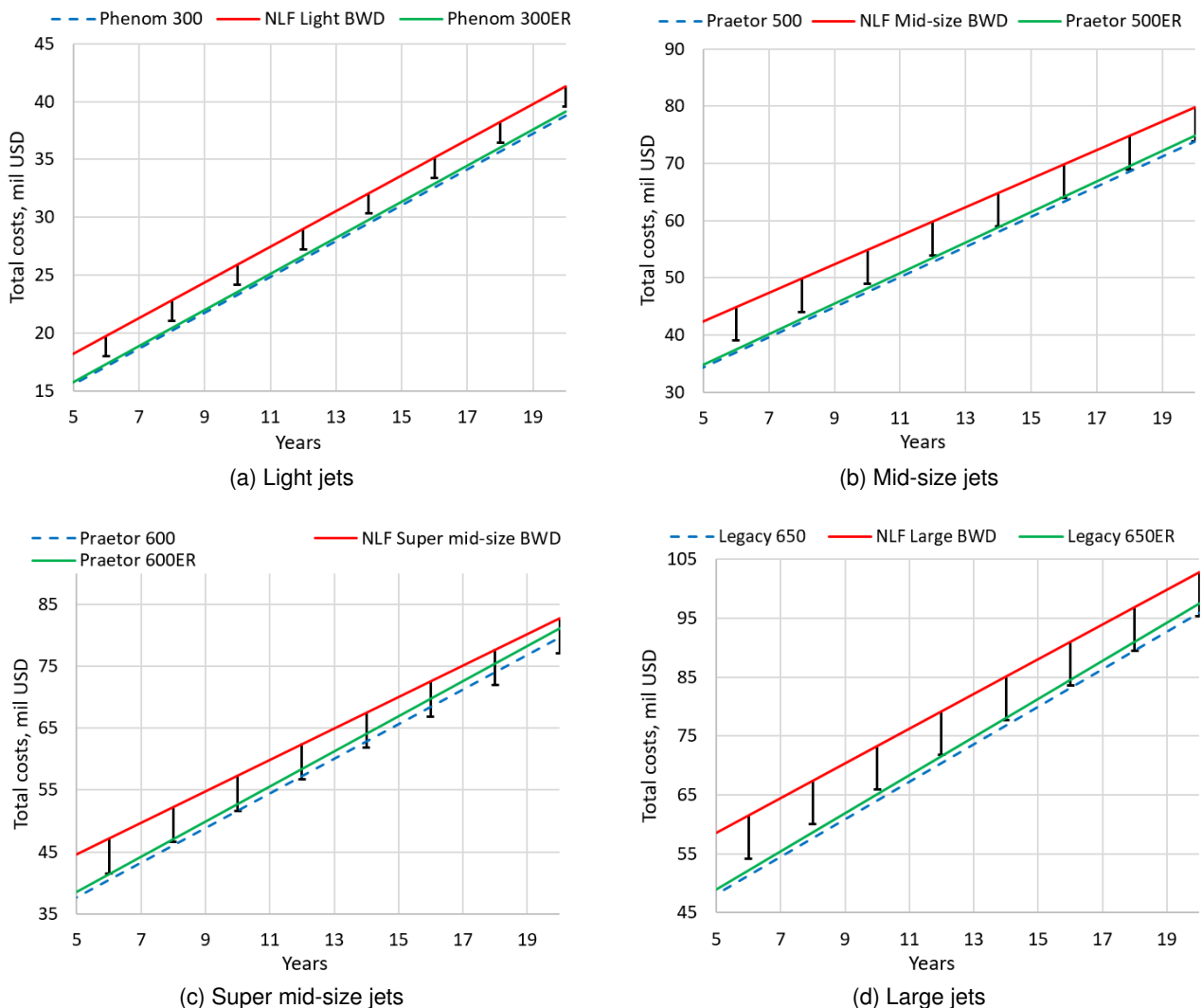
Figure 20 – Operating costs comparison for reference, extended reference, and designed aircraft for 750 flight hours/year.

investigate aircraft economic impact of NLF technologies, operating costs over a period of time for a fixed number of flight hours shall be investigated. For each market segments, three aircraft are compared: the benchmark reference aircraft, the reference aircraft with an extended range (ER) to approach the productivity and range performance of the NLf aircraft, and the NLF backward-swept

version since its price is the cheapest. A more optimistic value of flight hours of 750 hours/year is taken to model operations of charter companies. In addition, if a more optimistic value demonstrates optimistic results, lower flight hours values can be used. Finally, a more optimistic lower bound of the development difficulty factor 0f 1.2 (compared to the baseline 1.5 and 1.0 for aluminium aircraft) is taken as a bound of a virtual case when technology development reaches relatively high maturity. The material factor of 1.33 for development costs was taken as an optimistic scenario of material costs improvements.

Figure 20 summarizes operating costs comparisons among prescribed aircraft in each market segment. Solid red lines represent NLF aircraft costs with baseline assumptions considered for the design while error bars represent cost reduction due to potential technology maturity. Green lines present reference aircraft with a range extension to match the NLF aircraft range as an easier alternative to improve the aircraft PI. Blue dashed lines represent the reference aircraft. As expected, a simple range extension of the reference aircraft lead to increase in operating costs. However, the increase varies with the market segment. As for NLF aircraft, light jets do not demonstrate any financial benefit compared to reference aircraft even even with costs reduction factors. The situation improves for mid-size jets but does not present any significant financial benefits. For super mid-size and large jets, costs profiles show more potential. While the super mid-size baseline costs do not outperform reference aircraft within 20 years, maturity in design methodologies may lead to financial benefits after six years of aircraft operations. For the large jets, the trend was more conservative due to higher overall production costs. Since the development cost model directly depends on the aircraft empty weight, the increase in price magnitude is stronger for heavier aircraft. Consequently, a smaller aircraft (up to 12 passengers) which flies for relatively long distances may be a promising market segment for NLF technologies from costs perspective. However, it is important to note that the the design and development process must be mature enough to be able to achieve operating costs benefits. Moreover, if flight hours per year reduce from 750 to 450, actual costs benefit will happen not in six, but in ten years which may not be as short as desired by either a private owner or a charter airline. Contrary, if the aircraft manages to have achieve more flight hours per year, NLF benefits will become more significant. Other market segment do not show any improvements potential due to either insufficient reduction in DOC/hr (in case of light and mid-size jets) or a substantial increase in the aircraft base price (the large jet case).

7. Conclusion

Present work investigated the potential market applicability of natural laminar flow technologies for business jets. To perform the assessment, a database of twenty-eight existing business jets has been generated to answer the question of what parameters of the PI index show the highest sensitivity for each market segment from light to large jets. The regression analysis indicated that the range extension generally plays the second important role after the increase in speed, so the range increase is a strong market driver. This outcome motivated us to investigate how much NLF can extend an aircraft range without an increase in Direct Operating costs per year.

To quantify the potential of NLF aircraft, multiple configurations for each market segment have been sized. SUAVE initial sizing and MDO capabilities were used to size various aircraft configurations for each market. The SUAVE-embedded weights estimation method of FLOPS was calibrated to improve the weight estimation accuracy. DOC and price estimation methods were validated to ensure adequate estimations for designed aircraft. In addition, aircraft acquisition prices with an account of technological and material complexities factors were obtained. Results demonstrated the range extension between 5% and 15% depending on the aircraft configuration and market segment. Due to the implementation of NLF, acquisition prices for each aircraft increased. The least price growth was demonstrated by the backward-swept configuration due to the combination of NLF and weight reduction using composite materials for the wing. Based on obtained designs and costs analysis, only the class of super mid-size jets may benefit from the NLF technology from both performance and costs perspectives. Other market segments have significant increases in development costs and insufficient improvements in DOC. However, to achieve any benefit, development technologies and design experience must be mature enough to reduce development costs even for the conventional aircraft configuration.

Several questions remain open. First, the ultra-long-range jet market has not been considered and needs assessment. It is unknown how applicable the NLF technology is to the ultra-long-range jet market segment and what configuration may benefit the aircraft the most when the size of the aircraft approaches a commercial mid-range aircraft with cruise Mach numbers of 0.85 and more. Second, a high level of uncertainty due to development complexities assumptions and material costs remain and must be assessed separately to ensure prediction accuracy and draw more accurate conclusions. Finally, more information about the customer interest is required to ensure that the potential customer interest obtained in the present work models real needs or real customers.

Appendix

Table 8 – Geometric characteristics of NLF light business jets.

Parameter	Light BWD-swept wing	Light BWD-swept wing wing engines	Units
Wing			
Aspect ratio	7.38	7.00	-
Span	14.08	14.61	m
taper ratio	0.39	0.36	-
Quarter-chord sweep	20.21	-22.17	deg
Leading edge sweep	23.16	-19.00	deg
Dihedral	3.0	8.00	deg
Root thickness	12.0	11.0	%
Tip thickness	10.7	9.5	%
Horizontal tail			
Tail volume ratio	0.81	0.81	-
Span	5.26	6.05	m
taper ratio	0.53	0.53	-
Root chord	1.60	1.85	m
Leading edge sweep	25.0	25.0	deg
Thickness	10.0	10.0	%
Vertical tail			
Tail volume ratio	0.064	0.064	
Span	2.02	2.25	m
taper ratio	0.63	0.63	-
Root chord	2.70	3.00	m
Leading edge sweep	45	45	deg
Thickness	10.0	10.0	%

Table 9 – Designed light aircraft weights break-down.

Parameter	Light BWD-swept wing	Light BWD-swept wing wing engines	Units
Maximum take-off weight	7631	7585	kg
Maximum zero-fuel weight	5276	5293	kg
Operating empty weight	4756	4773	kg
Maximum Payload	1096	1096	kg

Table 10 – Geometric characteristics of NLF mid-size business jets.

Parameter	Mid-size BWD-swept wing	Mid-size FWD-swept wing	Mid-size FWD-swept wing mid-wing	Units
Wing				
Aspect ratio	8.58	8.00	8.19	-
Span	20.15	19.13	19.58	m
taper ratio	0.31	0.31	0.31	-
Quarter-chord sweep	27.3	-23.3	-23.4	deg
Leading edge sweep	30.0	-20.0	-20.0	deg
Dihedral	3.0	8.00	6.00	deg
Root thickness	11.7	11.7	11.7	%
Tip thickness	9.6	9.5	9.6	%
Horizontal tail				
Tail volume ratio	0.93	0.93	0.93	-
Span	8.71	8.48	8.95	m
taper ratio	0.60	0.60	0.60	-
Root chord	1.97	2.02	2.13	-
Leading edge sweep	28.0	28.0	28.0	deg
Thickness	10.0	10.0	10.0	%
Vertical tail				
Tail volume ratio	0.085	0.085	0.085	-
Span	3.78	3.78	4.05	m
taper ratio	0.54	0.54	0.54	-
Root chord	4.35	4.35	4.66	m
Leading edge sweep	48.0	48.0	48.0	deg
Thickness	10.0	10.0	10.0	%

Table 11 – Designed mid-size aircraft weights break-down.

Parameter	Mid-size BWD-swept wing	Mid-size FWD-swept wing	Mid-size FWD-swept wing mid-wing	Units
Maximum take-off weight	16420	16874	16728	kg
Maximum zero-fuel weight	10624	10935	10934	kg
Operating empty weight	9897	10208	10207	kg
Maximum Payload	1325	1325	1325	kg

Table 12 – Geometric characteristics of NLF super mid-size business jets.

Parameter	Super mid-size BWD-swept wing	Super mid-size FWD-swept wing	Super mid-size FWD-swept wing mid-wing	Units
Wing				
Aspect ratio	8.5	8.00	8.00	-
Span	21.05	20.87	20.68	m
taper ratio	0.35	0.25	0.27	-
Quarter-chord sweep	27.5	-23.7	-23.5	deg
Leading edge sweep	30.0	-20.0	-20.0	deg
Dihedral	3.0	8.00	6.0	deg
Root thickness	11.8	11.7	11.7	%
Tip thickness	10.5	9.5	9.3	%
Horizontal tail				
Tail volume ratio	0.92	0.92	0.92	-
Span	9.05	9.94	10.22	m
taper ratio	0.50	0.50	0.50	-
Root chord	2.23	2.45	2.52	m
Leading edge sweep	28.0	28.0	28.0	deg
Thickness	10.0	10.0	10.0	%
Vertical tail				
Tail volume ratio	0.092	0.092	0.092	
Span	7.18	6.75	6.08	m
taper ratio	0.54	0.54	0.54	-
Root chord	4.19	4.40	4.57	m
Leading edge sweep	48.0	48.0	48.0	deg
Thickness	10.0	10.0	10.0	%

Table 13 – Designed super mid-size aircraft weights break-down.

Parameter	Super mid-size BWD-swept wing	Super mid-size FWD-swept wing	Super mid-size FWD-swept wing mid-wing	Units
Maximum take-off weight	18763	18903	19046	kg
Maximum zero-fuel weight	10676	10862	11041	kg
Operating empty weight	10676	10862	11660	kg
Maximum Payload	1497	1497	1497	kg

Table 14 – Geometric characteristics of NLF large business jets.

Parameter	Large BWD-swept wing	Large FWD-swept wing	Units
Wing			
Aspect ratio	8.11	8.1	-
Span	20.83	21.3	m
taper ratio	0.33	0.26	-
Quarter-chord sweep	27.2	-23.5	deg
Leading edge sweep	30.0	-20.0	deg
Dihedral	3.0	6.0	deg
Root thickness	11.0	11.0	%
Tip thickness	9.5	9.8	%
Horizontal tail			
Tail volume ratio	0.96	0.96	-
Span	8.65	8.94	m
taper ratio	0.6	0.6	-
Root chord	2.35	2.43	-
Leading edge sweep	22.0	22.0	deg
Thickness	10.0	10.0	%
Vertical tail			
Tail volume ratio	0.078	0.078	
Span	3.51	3.51	m
taper ratio	0.56	0.56	-
Root chord	3.55	3.55	m
Leading edge sweep	35.0	47	deg
Thickness	10.0	10.0	%

Table 15 – Designed large aircraft weights break-down.

Parameter	Large BWD-swept wing	Large FWD-swept wing	Units
Maximum take-off weight	23000	23219	kg
Maximum zero-fuel weight	14146	14547	kg
Operating empty weight	13350	13751	kg
Maximum Payload	2240	2240	kg

Table 16 – Designed light aircraft Performance characteristics.

Parameter	Light BWD-swept wing	Light BWD-swept wing wing engines	Units
Maximum sea-level thrust	33.6	30.6	kN
Range (4 PAX, max fuel)	4163	4118	km
Maximum cruise Mach	0.80	0.80	-
TOFL	932	955	m
Landing distance	643	537	m

Table 17 – Designed mid-size aircraft Performance characteristics.

Parameter	Mid-size BWD-swept wing	Mid-size FWD-swept wing	Mid-size FWD-swept wing mid-wing	Units
Maximum sea-level thrust	62.9	65.9	65.4	kN
Range (4 PAX, max fuel)	6748	6692	6490	kg
Maximum cruise Mach	0.81	0.81	0.81	-
TOFL	1265	1285	1285	m
Landing distance	528	527	576	m

Table 18 – Designed super mid-size aircraft Performance characteristics.

Parameter	Super mid-size BWD-swept wing	Super mid-size FWD-swept wing	Super mid-size FWD-swept wing mid-wing	Units
Maximum sea-level thrust	71.5	70.5	73.3	kN
Range (4 PAX, max fuel)	8477	8536	8253	km
Maximum cruise Mach	0.81	0.81	0.81	-
TOFL	1267	1352	1281	m
Landing distance	535	531	602	m

Table 19 – Designed large aircraft Performance characteristics.

Parameter	Large BWD-swept wing	Large FWD-swept wing	Units
Maximum sea-level thrust	76.4	76.4	kN
Range (4 PAX, max fuel)	8162	8005	km
Maximum cruise Mach	0.8	0.8	m
TOFL	1716	1700	m
Landing distance	733	708	kg

8. Contact Author Email Address

Karpuk: s.karpuk@tu-braunschweig.de. Elham: a.elham.tu-braunschweig.de

9. Copyright Statement

References

[1] Isikveren A, Goritschnig G and Noel M. Productivity Metrics for Business and Regional Aircraft. *SAE Technical Paper*, 2003-01-3063, 2003.

[2] Hepperle M. MDO of Forward Swept Wings. *In Proceedings of the KATnet II Workshop*, 28 − 29 Jan 2008, Braunschweig, Germany.

[3] Schrauf G and Geyr H. Simplified Hybrid Laminar Flow Control for the A320 Fin - Aerodynamic and System Design, First Results. *AIAA Scitech 2020 Forum*, Orlando, FL, USA.

[4] Holmes B, Obara C, Martin G and Domack, C. Manufacturing Tolerances for natural Laminar Flow Airframe Surfaces. *SAE Technical Paper*, 850863, 1985.

[5] Steffen O, Buggisch M, Kappel E, Köke H, Meyer P and Hühne C. Flight Testing on Ground - The Laminar Wing Leading Edge Ground Based Demonstrator. *Deutscher Luft- und Raumfahrtkongress DLRK 2019*, Darmstadt, Germany, 12 Sept − 2 Oct 2019.

[6] Heinrich L and Kruse M. Laminar Composite Wing Surface Waviness - Two Counteracting Effects and a Combined Assessment by Two Methods. *Deutscher Luft- und Raumfahrtkongress 2016*, 13 − 15 Sept 2016, Braunschweig, Germany.

[7] Wunderlich T and Dähne S. Aeroelastic tailoring of an NLF forward swept wing : DLR contribution to LuFo IV joint research project AeroStruct, *CEAS Aeronautical Journal*, Vol. 8, 3, 2017.

[8] Nangia A. Forward swept wings and Application in high aspect ratio aircraft configurations. *Symposium organized by the Netherlands Association of Aeronautical Engineers (NVvL) and the Students Society 'Leonardo da Vinci'*, Delft, Netherlands, April 24, 1987.

[9] Seitz A, Hübner A and Risse K. The DLR TuLam project: design of a short and medium range transport aircraft with forward swept NLF wing, *CEAS Aeronaut Journal*, Vol. 11, 2020.

[10] Steffen O, Buggisch M, Kappel E, Köke H, Meyer P and Hühne C. Flight Testing on Ground - The Laminar Wing Leading Edge Ground Based Demonstrator. *Deutscher Luft- und Raumfahrtkongress DLRK 2019*, Darmstadt, Germany, 30 Sept - 2 Oct 2019.

[11] Annex 6 to the Convention on International Civil Aviation, Operation of Aircraft, Part 1. *International Commercial Air Transport - Aeroplanes*, 2013.

[12] Certification Specifications and Acceptable Means of Compliance for Large Aeroplanes CS-25, EASA, 2020.

[13] Fujino M. Design and Development of the HondaJet, *Journal of Aircraft*, Vol. 42, 3, 2005.

[14] McDonald R. Advanced modeling in OpenVSP. *16th AIAA Aviation Technology, Integration, and Operations Conference*, 13–17 June 2016, Washington, D.C., USA.

[15] Lukaczyk T, Wendroff A, Colonno M, Economon T, Alonso J, Orra T and Ilario C. SUAVE: An Open-Source Environment for Multi-Fidelity Conceptual Vehicle Design. *In Proceedings of the 16th AIAA ISSMO Multidisciplinary Analysis and Optimization Conference*, Dallas, TX, USA, 22–26 June 2015.

[16] Gudmundsson S. *General Aviation Aircraft Design: Applied Methods and Procedures*, 1st ed, Butterworth-Heinemann: Oxford, UK, 2013.

[17] Raymer D. *Aircraft Design: A Conceptual Approach*, 6th ed, American Institute of Aeronautics and Astronautics: Washington, DC, USA, 2018.

[18] Torenbeek E. *Synthesis of Subsonic Airplane Design*; Springer: Delft, The Netherlands, 1982.

[19] Roskam J. *Airplane Design*, 2nd ed, Darcorporation, Lawrence, KS, USA, 2003.

[20] Hoelzen J, Liu Y, Bensmann B, Winnefeld C, Elham A, Friedrichs J and Hanke-Rauschenbach R. Conceptual Design of Operation Strategies for Hybrid-Electric Aircraft, *Energies*, Vol.11, 1, **2018**.

[21] Scholz D. Aircraft Design - an Open Educational Resource (OER) for Hamburg Open Online University (HOOU),Wing Design, 2015.

[22] Andersson J and P Krus P. A Multi-Objective Optimization Approach to Aircraft Preliminary Design. *SAE 2003 Transactions Journal of Aerospace*, Vol. 112, 1, 2003.

[23] Wells D, Horvath B and McCullers L. The Flight Optimization System Weights Estimation Method. NASA TM 20170005851, NASA: Hampton, Virginia, 2017.

[24] Franz K. CeRAS Direct Operating Cost (DOC) Model; RWTH Aachen University, 2014.

[25] Getting Hands-on Experience with Aerodynamic Deterioration, A Performance Audit View. Airbus, Issue 2, 2001.

[26] Dutton S, Kelly, D and Baker A. *Composite Materials for Aircraft Structures.* 2nd ed, American Institute of Aeronautics and Astronautics: Washington, DC, USA, 2012.

[27] Global Air. Aviation fuel price statistics.

[28] Compare Private Planes, Online aircraft database.

[29] General Aviation Manufacturers Association, 2018 Annual Report, 2018.

[30] Air.one; Online aircraft database.

[31] Carichner G and Nicolai L. *Fundamentals of Aircraft and Airship Design, Volume 2 – Airship Design and Case Studies*. American Institute of Aeronautics and Astronautics: Washington, DC, USA, 2013.

[32] Weiland M. Low Cost Manufacturing and Assembly of Composite and Hybrid Structures, Linköping, Sweden, 2016.

[33] Kruse M, Wunderlich T and Heinrich L. A Conceptual Study of a Transonic NLF Transport Aircraft with Forward Swept Wings, *30th AIAA Applied Aerodynamics Conference*, New Orleans, Louisiana, USA, 25 – 28 June 2012.

[34] Meyer R and Anderson B. Effects of Wing Sweep on In-flight Boundary-layer Transition for a Laminar Flow Wing at Mach Numbers from 0.60 to 0.79. NASA TM-101701, NASA Ames: Edwards, Ca, USA, 1990.

[35] Meyer R and Anderson B. Effects of Wing Sweep on Boundary-layer Transition for a Smooth F-14A Wing at Mach Numbers from 0.700 to 0.825. NASA TM-101712, NASA Ames: Edwards, Ca, USA, 1990.

[36] Sweptforward Wings for the HFB 320 Hansa: An Outline of the Design Considerations which Led to the Adoption of Sweptforward Wings for the Hamburger Flugzeugbau Hansa Jet Executive Aircraft, *Aircraft Engineering and Aerospace Technology*, Vol. 36, 8, 1964.